Macromolecules
Cite This: Macromolecules 2019, 52, 1173−1187
Article
pubs.acs.org/Macromolecules

# Preparation and Controlled Degradation of Model Amphiphilic Long-Subchain Hyperbranched Copolymers: Hyperblock versus Hypergraft

Jinxian Yang,[†,§] Yixia Li,[†] Nairong Hao,[†] Ahmad Umair,[†] Anhong Liu,[†] Lianwei Li,*[,†] and Xiaodong Ye*[,†,‡]

[†]Hefei National Laboratory for Physical Sciences at the Microscale, Department of Chemical Physics, and [‡]CAS Key Laboratory of Soft Matter Chemistry, University of Science and Technology of China, Hefei, Anhui 230026, China

[§]Shenzhen Key Laboratory for Functional Polymer, School of Chemistry and Chemical Engineering, Shenzhen University, Shenzhen, Guangdong 518060, China

Supporting Information

**ABSTRACT:** The controlled degradation of amphiphilic hyperbranched polymers (AHPs) is the first consideration for their bio-related applications. In this contribution, we aim to get some insight into the effect of block distribution and composition on the degradation behavior of AHPs model systems. Degradable amphiphilic hyperbranched block (Hyperblock) and graft (Hypergraft) copolymers with hydrophobic poly(ε-caprolactone) (PCL) and hydrophilic poly[tri(ethylene glycol) methyl ether acrylate] (PTEGMA) as building blocks were prepared in this study, i.e., HB-PCL-*b*-PTEGMA and HB-PCL-*g*-PTEGMA. The two kinds of AHPs own cleavable disulfide linkages embedded at all branching sites. Their degradation behavior was comparatively investigated in aqueous solutions. The results reveal that the block distribution and composition play different roles in the regulation of degradation behavior of long-subchain hyperbranched self-assembly amphiphiles (SAs). Namely, the degradation process is mainly affected by chain architecture of resultant SAs, while for a given architecture, the degradation rate can be regulated by systematically varying the block composition.

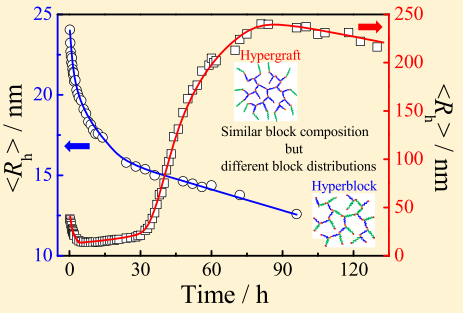


## INTRODUCTION

As one main subclass of dendritic polymers, hyperbranched polymers (HPs) have received increasing attention in the past two decades because of their unique properties, such as facile synthesis,[1−4] good solubility,[5] low viscosity,[6] and high number of terminal functional groups.[3,7] These advantages have led to wide use of HPs as functional materials in various applications, such as biomedical materials,[4,8−15] polymer coating materials,[16] optoelectronic materials,[17,18] and so forth. Accordingly, numerous efforts have been devoted to the understanding of the structure−property relationship for HPs in different applications.

Among the various applications mentioned above, the development of amphiphilic hyperbranched polymer (AHP)-based encapsulating/framework materials for nanomedicine application is one of the hottest topics and has been extensively studied in the past decade. Namely, Yan et al.[19] studied the self-assembly and redox-responsive property of polyphosphate-based AHPs. Kim et al.[20] designed a double hydrophilic hyperbranched copolymer made of poly(ethylene oxide) and polyglycerol and found that the assembled micelles can exhibit a pH-responsive release of doxorubicin (DOX). Liu et al.[21] prepared hyperbranched unimolecular poly-prodrug micelles for synergistic reductive milieu-triggered drug release and enhanced magnetic resonance signals. Clearly, all these examples demonstrate the great potential of using HPs as eco-friendly functional materials in bio-related applications. Nevertheless, a careful literature search shows that only a limited understanding of the structure−property relation for AHPs has been achieved. It is yet to be found that how the molecular parameters of AHPs, such as the molar mass, molar mass distribution, degree of branching, and the hydrophilicity/hydrophobicity balance, affect the framework degradation, small-molecule loading efficiency, and release behavior of AHP-based self-assembly amphiphiles (SAs) in aqueous solutions.[22,23] This is mainly attributed to the uncontrollability of structural parameters of prepared HPs in previous reports.[20,24]

So far, two major synthetic approaches have been developed for the preparation of HPs including the chain-growth polymerization and step-growth polymerization strategies. Because of the synthetic facilitation, the chain-growth polymerization methods, including self-condensing vinyl polymerization (SCVP)[25−27] and self-condensing ring-opening polymerization (SCROP),[28,29] have been widely used for the preparation of HPs. Even the synthetic methods could offer

Received: August 17, 2018
Revised: January 6, 2019
Published: January 29, 2019







DOI: 10.1021/acs.macromol.8b01784
Macromolecules 2019, 52, 1173−1187

**Scheme 1. Schematic Illustration of Topological Structures of Prepared (a) Hyperblock and (b) Hypergraft Amphiphilic Copolymers**

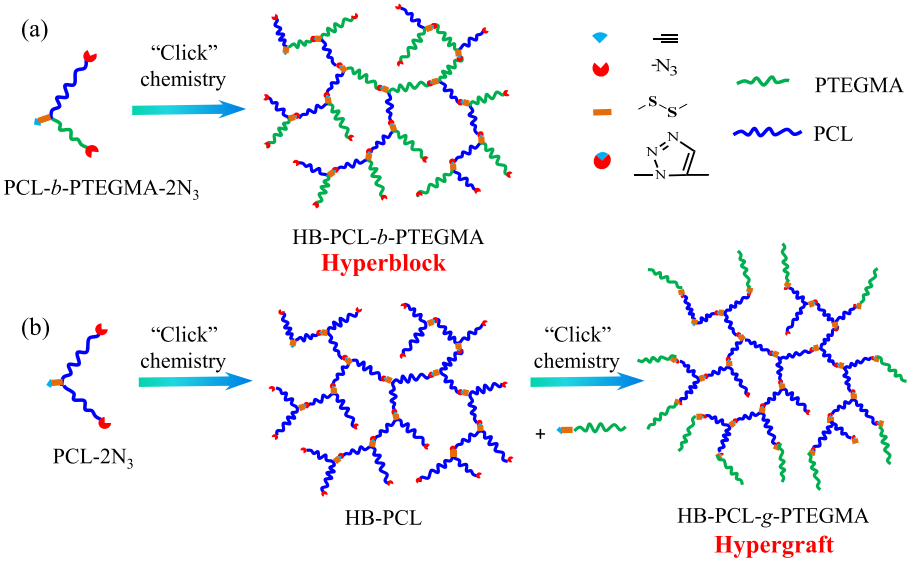


moderate control over the chain parameters such as the molar mass and the average branching subchain length, while the subchain length distribution is still less controlled, which partially explains why the previously established structure–property relationships generally lack the universality and could hardly be applied to different systems. In contrast, the step-growth polymerization approach has shown a much better control over these chain parameters.[30] Recently, we proposed a novel seesaw-type $AB_2$ macromonomer strategy for the preparation of HPs with uniform and controlled subchains,[31,32] where the subchain length is exactly half of initial macromonomer length. Our systematic investigations have revealed that various solution properties of resultant HPs are strongly dependent on the internal subchain length.[33−35] Moreover, using model hyperbranched polystyrene chains with both uniform subchains and controlled locations of cleavable disulfide linkage,[36] we quantitatively investigated their degradation behavior in THF, and the results highlighted the importance of controlled locations of cleavable disulfide linkages for model degradation.

For a real AHP nanocarrier system, loading efficiency, degradation rate of polymer framework, drug release rate, and biocompatibility are the critical factors to be considered while designing the structure of AHP nanocarriers. On the other hand, all the properties are mainly correlated to the molecular parameters, such as the overall molar mass, polydispersity, number and distribution of branching subchains and degradation sites, and block sequence. It is no exaggeration to say that the preparation of model AHP systems with controlled branching subchains and degradation sites, as well as well-defined distribution pattern and composition of hydrophobic/hydrophilic blocks, is the prerequisite for further regulating the related property of AHPs-based nanocarrier system.

For the proof of concept, we prepared two hyperbranched polymer model systems (Hyperblock and Hypergraft) for the comparative study of the influence of block distribution and composition on the degradation behavior of AHP SAs in aqueous solutions, where the biocompatible poly(ε-caprolactone) (PCL) and poly[tri(ethylene glycol) methyl ether acrylate] (PTEGMA) were used as hydrophobic and hydrophilic blocks, respectively (Scheme 1). For Hyperblock, it was made from PCL-*b*-PTEGMA diblock macromonomer, and the inserted hydrophobic and hydrophilic blocks were randomly distributed in the resultant Hyperblock structure, while Hypergraft was made of a hydrophobic hyperbranched PCL core with hydrophilic PTEGMA chains grafted on the periphery. Based on our previously proposed synthetic approach, both model systems own controlled branching subchains and cleavable redox-sensitive disulfide bonds. Moreover, we first intentionally controlled the composition of hydrophobic/hydrophilic blocks of Hyperblock and Hypergraft copolymers to be similar to each other to study the effect of block distribution. In addition, for a given architecture, hyperbranched copolymers with varied block length were also prepared to study the effect of block composition. Thus, the two model systems afford us the opportunity, *for the first time*, to elucidate how the block distribution and composition influence the degradation of amphiphilic long-subchain HPs in aqueous solutions. Experimentally, a significantly different degradation behavior was observed for the two AHPs systems, highlighting the importance of the rational design of block distribution and composition for AHPs in different applications. The results simultaneously demonstrate that both of the model systems are potential candidates as nanocarriers for practical nanomedicine application.

## MATERIALS

ε-Caprolactone (CL, Aladdin, 99%) was dried over calcium hydride and distilled under reduced pressure. Copper(I) bromide (CuBr, Alfa Aesar, 98%) was washed with glacial acetic acid to remove soluble oxidized species, filtrated, washed with ethanol, and dried under vacuum. Acetonitrile (ACN, Sinopharm, 99%) and triethylamine (TEA, Sinopharm, 97%) were refluxed over *p*-toluenesulfonyl chloride and then distilled over calcium hydride prior to use. Dichloromethane (DCM, Sinopharm, 97%) was distilled over calcium hydride. Dimethylformamide (DMF, Sinopharm, 97%) was first dried with anhydrous magnesium sulfate and then distilled under reduced pressure. Tetrahydrofuran (THF, Sinopharm, 99%) and toluene (Sinopharm, 97%) were refluxed over sodium for 24 h and then distilled. 2-Bromopropionyl bromide (Aladdin, 97%), 2-bromoisobu-


DOI: 10.1021/acs.macromol.8b01784
Macromolecules 2019, 52, 1173−1187

**Scheme 2. Schematic Illustration of (a) Hyperblock Copolymer HB-PCL-*b*-PTEGMA and (b) Hypergraft Copolymer HB-PCL-*g*-PTEGMA**

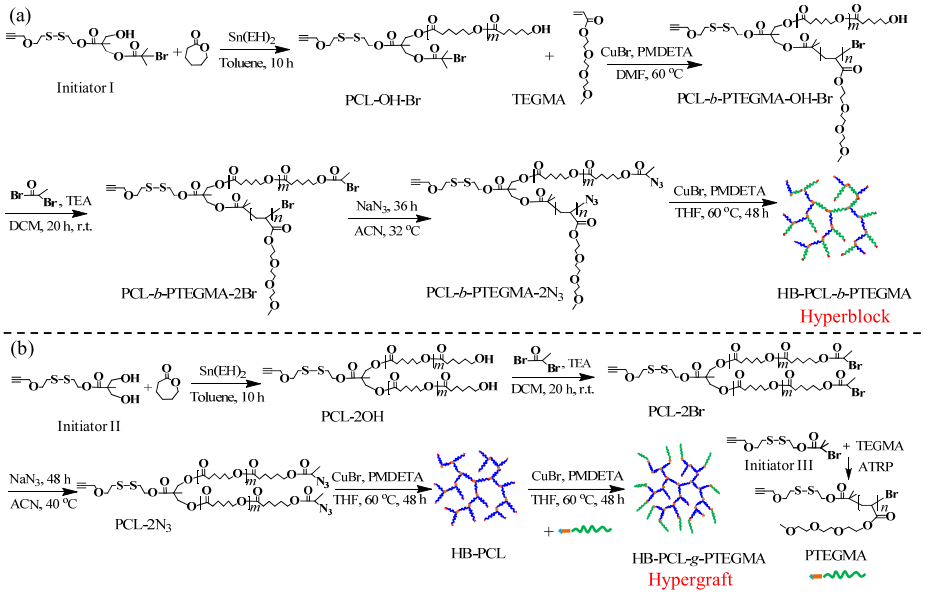


tyryl bromide (Aladdin, 98%), acryloyl chloride (Aladdin, 96%), triethylene glycol monomethyl ether (Sigma-Aldrich, 95%), sodium azide ($NaN_3$, Sigma-Aldrich, 99%), *N*,*N*,*N*′,*N*′,*N*″-pentamethyldiethylenetriamine (PMDETA, Sigma-Aldrich, 99%), tin(II) 2-ethylhexanoate ($Sn(EH)_2$, Sigma-Aldrich, 95%), and other analytical grade reagents from Sinopharm were used as received. The water used in this work is Milli-Q water (Millipore, resistivity = 18.2 MΩ·cm at 25 °C).

The synthesis of Hyperblock (HB-$PCL_{26}$-*b*-$PTEGMA_{12}$) and Hypergraft copolymer (HB-$PCL_{23}$-*g*-$PTEGMA_{13}$) is detailed as follows, as shown in Scheme 2, and the syntheses of other hyperbranched copolymers with different compositions are similar. The subscript number represents the degree of polymerization of the repeating unit calculated from $^1$H NMR, which will be discussed later.

**Synthesis of PCL-OH-Br by Ring-Opening Polymerization (ROP).** In a typical reaction, 0.67 g of initiator I (1.46 mmol), 4.01 g of ε-caprolactone (35.2 mmol), and 0.09 g of $Sn(EH)_2$ (0.22 mmol) were added into a 100 mL three-neck bottle, and then anhydrous toluene (50 mL) was added. The mixture was stirred for 10 h at 115 °C under an argon atmosphere. The solvent was removed by rotary evaporation after the reaction was stopped. The product was redissolved in THF and precipitated into an excess of cold methanol/water mixture (3/1, v/v). The precipitation process was repeated for three times. The white solid $PCL_{26}$-OH-Br was obtained after drying under vacuum at 40 °C for 24 h (yield: 4.0 g, 85%). $^1$H NMR chemical shift for $PCL_{26}$-OH-Br (δ, ppm, $CDCl_3$): 4.38−4.45 (−COO−$CH_2$−$CH_2$−SS−), 4.20−4.37 (−COO−$CH_2$−C−COO−), 4.18−4.20 (CH≡C−$CH_2$−), 4.00−4.12 (−OOC−$CH_2$−$CH_2$−$CH_2$−$CH_2$−$CH_2$−O−), 3.75−3.83 (−$CH_2$−O−$CH_2$−$CH_2$−SS−), 3.60−3.70 (−$CH_2$−$CH_2$−OH), 2.85−3.00 (−$CH_2$−$CH_2$−SS−$CH_2$−$CH_2$−), 2.43−2.52 (CH≡C−), 2.24−2.42 (−OOC−$CH_2$−$CH_2$−$CH_2$−$CH_2$−$CH_2$−O−), 1.65−1.87 (−OOC−C($CH_3$)$_2$−Br), 1.53−1.77 (−OOC−$CH_2$−$CH_2$−$CH_2$−$CH_2$−$CH_2$−O−), 1.27−1.48 (−OOC−$CH_2$−$CH_2$−$CH_2$−$CH_2$−$CH_2$−O−), 1.26−1.32 (−OOC−C−$CH_3$).

**Synthesis of PCL-*b*-PTEGMA-OH-Br by Atom Transfer Radical Polymerization (ATRP).** Tri(ethylene glycol) methyl ether acrylate (TEGMA) was synthesized according to the reported procedure.[37] 1.6 g of $PCL_{26}$-OH-Br (0.47 mmol), 5.10 g of TEGMA (23.4 mmol), 100 μL of PMDETA (0.48 mmol), and anhydrous DMF (5 mL) were added into a 20 mL glass tube with a magnetic stirrer. After degassing by three freeze−vacuum−thaw cycles, 68 mg of CuBr (0.47 mmol) was added into the tube, and then the tube was sealed under vacuum. The mixture was stirred at 60 °C for 3 h. Then the mixture was diluted with THF and passed through a short neutral alumina column to remove the metal salt. The solvent was removed by rotary evaporation. The product was redissolved in THF and precipitated into an excess amount of cold *n*-hexane. The precipitation process was repeated for three times. The white solid $PCL_{26}$-*b*-$PTEGMA_{12}$-OH-Br was obtained after drying under vacuum at 40 °C for 24 h (yield: 2.2 g, 74%).

**Synthesis of PCL-*b*-PTEGMA-2Br by Functional Modification.** 2.05 g of $PCL_{26}$-*b*-$PTEGMA_{12}$-OH-Br (0.34 mmol), 0.34 g of TEA (3.4 mmol), and anhydrous DCM (30 mL) were added into a 50 mL three-neck bottle. 0.73 g of 2-bromopropionyl bromide (3.4 mmol) dissolved in anhydrous DCM (5 mL) was added dropwise within 1 h at 0 °C. The mixture was stirred for 20 h at room temperature under an argon atmosphere. The solvent was removed by rotary evaporation after the reaction was stopped. The residue was redissolved in THF. After the removal of insoluble salts by filtration, the filtrate was concentrated by a rotary evaporator. The polymer solution was precipitated into an excess amount of cold *n*-hexane. The precipitation process was repeated three times. The light yellow solid $PCL_{26}$-*b*-$PTEGMA_{12}$-2Br was obtained after drying under vacuum at 40 °C for 24 h (yield: 1.89 g, 92%).

**Synthesis of PCL-*b*-PTEGMA-2$N_3$ by Azidation.** 1.84 g of $PCL_{26}$-*b*-$PTEGMA_{12}$-2Br (0.30 mmol) was dissolved in ACN (20 mL), and then 0.59 g of $NaN_3$ (9.1 mmol) was added into the solution. The mixture was stirred at 32 °C for 36 h under an argon atmosphere. The solvent was removed by rotary evaporation after the reaction was stopped, and the product was redissolved in THF. After being centrifuged for 30 min × 3, the supernatant was precipitated into an excess amount of cold *n*-hexane. The light yellow solid $PCL_{26}$-*b*-$PTEGMA_{12}$-2$N_3$ was obtained after drying under vacuum at 40 °C for 24 h (yield: 1.6 g, 87%).

**Synthesis of Hyperblock Copolymer HB-PCL-*b*-PTEGMA by "Click" Reaction.** 1.55 g of $PCL_{26}$-*b*-$PTEGMA_{12}$-2$N_3$ (0.26 mmol), 96 μL of PMDETA (0.46 mmol), and THF (10 mL) were added into a 20 mL glass tube with a magnetic stirrer. After degassing by three freeze−vacuum−thaw cycles, 68 mg of CuBr (0.46 mmol) was added into the tube, and then the tube was sealed under vacuum. The mixture was stirred at 60 °C for 48 h. Then the mixture was diluted with THF and passed through a short neutral alumina column to remove the metal salt. After being concentrated, the polymer solution was precipitated into an excess amount of cold *n*-hexane. The solid HB-$PCL_{26}$-*b*-$PTEGMA_{12}$ was obtained after drying under vacuum at



DOI: 10.1021/acs.macromol.8b01784
*Macromolecules* 2019, 52, 1173−1187

40 °C for 24 h (yield: 1.1 g, 71%), and then the product was fractionated with *n*-hexane/THF mixture (1−1.5/1, v/v) (yield: 0.12 g, 11%).

**Synthesis of PCL-2OH by ROP.** In a typical reaction, 0.74 g of initiator II (2.4 mmol), 6.02 g of ε-caprolactone (52.8 mmol), and 0.20 g of $Sn(EH)_2$ (0.49 mmol) were added into a 100 mL three-neck bottle, and then anhydrous toluene (60 mL) was added. The mixture was stirred for 10 h at 115 °C under an argon atmosphere. The solvent was removed by rotary evaporation after the reaction was stopped. The product was redissolved in THF and precipitated into an excess of cold methanol/water mixture (3/1, v/v). The precipitation process was repeated for three times. The white solid $PCL_{23}$-2OH was obtained after drying under vacuum at 40 °C for 24 h (yield: 6.1 g, 90%).

**Synthesis of PCL-2Br by Functional Modification.** 5.8 g of $PCL_{23}$-2OH (2.0 mmol), 2.51 g of TEA (24.9 mmol), and 60 mL of anhydrous DCM were added into a 100 mL three-neck bottle. A solution of 5.34 g of 2-bromopropionyl bromide (24.7 mmol) in anhydrous DCM (10 mL) was added dropwise within 1 h at 0 °C. The mixture was stirred for 20 h at room temperature under an argon atmosphere. The solvent was removed by rotary evaporation after the reaction was stopped. The residue was redissolved in THF. After the removal of insoluble salts by filtration, the filtrate was concentrated by a rotary evaporator. The polymer solution was precipitated into an excess amount of cold *n*-hexane. The precipitation process was repeated for three times. The light yellow solid $PCL_{23}$-2Br was obtained after drying under vacuum at 40 °C for 24 h (yield: 4.5 g, 78%).

**Synthesis of PCL-2$N_3$ by Azidation.** 2.3 g of $PCL_{23}$-2Br (0.78 mmol) was dissolved in ACN (20 mL), and then 1.4 g of $NaN_3$ (21.5 mmol) was added into the solution. The mixture was stirred at 40 °C for 48 h under an argon atmosphere. The solvent was removed by rotary evaporation after the reaction was stopped, and the product was redissolved in THF. After being centrifuged for 30 min × 3, the supernatant was precipitated into an excess of cold methanol/water mixture (3/1, v/v). The light yellow solid $PCL_{23}$-2$N_3$ was obtained after drying under vacuum at 40 °C for 24 h (yield: 1.3 g, 57%).

**Synthesis of PTEGMA by ATRP.** 0.78 g of initiator III (2.3 mmol), 7.02 g of TEGMA (32.2 mmol), 480 μL of PMDETA (2.30 mmol), and anhydrous DMF (5 mL) were added into a 20 mL glass tube with a magnetic stirrer. After degassing by three freeze−vacuum−thaw cycles, 230 mg of CuBr (1.6 mmol) was added into the tube, and then the tube was sealed under vacuum. The mixture was stirred at 60 °C for 3 h. Then the mixture was diluted with THF and passed through a short neutral alumina column to remove the metal salt. The solvent was removed by rotary evaporation. The product was redissolved in THF and precipitated into an excess amount of cold *n*-hexane. The precipitation process was repeated for three times. The transparent liquid $PTEGMA_{13}$ was obtained after drying under vacuum at 40 °C for 24 h (yield: 3.1 g, 47%). $^1$H NMR chemical shift for $PTEGMA_{13}$ (δ, ppm, $CDCl_3$): 4.25−4.45 ($CH{\equiv}C-CH_2-$, $-COO-CH_2-CH_2-SS-$, $-COO-CH_2-CH_2-O-$), 3.75−3.84 ($-O-CH_2-CH_2-SS-$), 3.60−3.74 ($-COO-CH_2-CH_2-O-CH_2-CH_2-O-CH_2-CH_2-O-$), 3.50−3.60 ($-O-CH_2-CH_2-O-CH_3$), 3.29−3.43 ($-O-CH_3$), 2.85−3.00 ($-CH_2-CH_2-SS-CH_2-CH_2-$), 2.47−2.56 ($CH{\equiv}C-$), 2.20−2.47 ($-CH_2-CH-COO-$), 1.38−2.15 ($-CH_2-CH-COO-$), 1.05−1.21 ($-C(CH_3)_2-COO-$).

**Synthesis of Hypergraft Copolymer HB-PCL-*g*-PTEGMA.** 1.2 g of $PCL_{23}$-2$N_3$ (0.41 mmol), 180 μL of PMDETA (0.86 mmol), and THF (6 mL) were added into a 20 mL Schlenk bottle. After degassing by three freeze−vacuum−thaw cycles, 120 mg of CuBr (0.83 mmol) was added immediately. 1.2 mL of hyperbranched PCL (HB-$PCL_{23}$) solution was taken out after the mixture was stirred at 60 °C for 48 h. Then a degassed polymer solution containing 3.0 g of $PTEGMA_{13}$ (9.4 mmol) was added into the Schlenk bottle, and the reaction was continued at 60 °C for another 48 h to get HB-$PCL_{23}$-*g*-$PTEGMA_{13}$. The remaining HB-$PCL_{23}$ and HB-$PCL_{23}$-*g*-$PTEGMA_{13}$ polymer solutions were treated with a similar procedure; i.e., the solutions were first diluted with THF and passed through a short neutral alumina column to remove the metal salt. After being concentrated, the HB-PCL solution was precipitated into an excess of cold methanol/water mixture (3/1, v/v) while the HB-$PCL_{23}$-*g*-$PTEGMA_{13}$ solution was precipitated into an excess amount of cold *n*-hexane. The HB-$PCL_{23}$-*g*-$PTEGMA_{13}$ was further fractionated with *n*-hexane/THF mixture (1−1.5/1, v/v). The light green solid HB-$PCL_{23}$ (yield: 50 mg, 25%) and HB-$PCL_{23}$-*g*-$PTEGMA_{13}$ (yield: 0.2 g, 8.3%) were obtained after drying under vacuum at 40 °C for 24 h.

**Preparation of Bare Polymeric Self-Assembly Amphiphiles (SAs).** All the SAs were prepared with the same procedure, and all the copolymers used are fractionated samples. In a typical process, 5 mg of HB-$PCL_{26}$-*b*-$PTEGMA_{12}$ was dissolved in DMF (1 mL). The water (5 mL) was added immediately into this polymer solution under vigorous stirring. The solution was dialyzed against water for 24 h (molecular weight cutoff ∼14000 g/mol) after being stirred at room temperature for 1 h.

**Preparation of Doxorubicin (DOX) Loaded SAs.** The typical preparation procedure of DOX loaded SAs was described as follows. First, DOX solution with a concentration of 10 mg/mL was prepared by mixing 10 mg of DOX·HCl and 5 mol equiv of TEA in DMSO (1 mL). 5 mg of HB-$PCL_{26}$-*b*-$PTEGMA_{12}$ was dissolved in DMF, and 100 μL of DOX solution (10 mg/mL) was added. Then water (1 mL) was added immediately into the mixture under vigorous stirring. The solution was dialyzed against water for 24 h (molecular weight cutoff ∼14000 g/mol) after being stirred at room temperature for 1 h. The DOX loaded SAs solution was centrifuged for 10 min × 3 at 4000 rpm to remove unloaded DOX. The UV absorbance of the mixture (100 μL DOX loaded SAs solution mixed with 900 μL DMSO) at 485 nm was measured to determine the total loading of DOX.[38,39] A standard curve of DOX in DMSO was obtained by the UV−vis spectrophotometer at 485 nm (Figure S1). The drug loading content (DLC) and drug loading efficiency (DLE) were calculated according to the following formulas:[40]

$$\mathrm{DLC}\ (\%) = \frac{m_{\mathrm{DOX\ in\ micelles}}}{m_{\mathrm{polymer}} + m_{\mathrm{DOX\ in\ micelles}}} \times 100\% \quad (1)$$

$$\mathrm{DLE}\ (\%) = \frac{m_{\mathrm{DOX\ in\ micelles}}}{m_{\mathrm{DOX}}} \times 100\% \quad (2)$$

**Degradation of Hyperblock and Hypergraft Copolymers in THF.** 25 mg of Hyperblock or Hypergraft copolymer was dissolved into 50 mL of THF. The oxygen in the solution was removed by bubbling nitrogen for 1 h, and then ∼80 mg of DTT was added into the solution. The degradation processes were monitored at 25 °C by GPC.

**Drug Release Kinetics in Vitro.** The drug release was conducted at 37 °C in 20 mM PB buffer (pH 7.4, 10 mM DTT). Typically, drug loaded SAs solutions were added into a dialysis bag (molecular weight cutoff ∼14000 g/mol) and dialyzed against 20 mL of PB buffer. At predetermined time points, the old buffer solution containing DOX was taken out, and 20 mL of fresh buffer was added. The buffer solution was freeze-dried and dissolved in DMSO. The DOX content was measured by a UV−vis spectrophotometer at 485 nm. The cumulative release of DOX was calculated.

**Characterization.** $^1$H NMR measurements were conducted on a Bruker AV400NMR spectrometer. Deuterated chloroform ($CDCl_3$) was used as the solvent while tetramethylsilane (TMS) was used as an internal standard. The concentration of polymers was ∼20 g/L. FTIR spectra were performed on a Bruker VECTOR-22 IR spectrometer. The samples were prepared by the KBr disk method, and the spectra were collected at 64 scans with a spectral resolution of 4 $cm^{-1}$. The molar mass and polydispersity index (PDI = $M_w/M_n$) were determined by gel permeation chromatography (GPC, Waters 1515) equipped with three Waters Styragel columns (HR2, HR4, and HR6) and a refractive index detector (RI, Wyatt WREX-02). The column oven temperature was kept at 35 °C. THF was used as eluent, and the flow rate was set at 1.0 mL/min. Molar masses were calibrated with narrowly distributed linear polystyrene samples.

**Differential Scanning Calorimetry (DSC).** DSC was performed on a Q2000 differential scanning calorimeter from TA Instruments under a nitrogen flow rate of 100 mL/min. First, the sample was



DOI: 10.1021/acs.macromol.8b01784
*Macromolecules* 2019, 52, 1173−1187

heated from −90 to 150 °C to remove the thermal history, and then the sample was reheated after cooling from 150 to −90 °C. The scanning rate was set at 10 °C/min. The endothermic maximum temperature during reheating was taken as the melting temperature ($T_m$). The degree of crystallinity ($\chi_c$) was calculated according to the equation as follows:[41,42]

$$\chi_c = \Delta H_m/(W_{PCL} \times \Delta H_{m,0}) \quad (3)$$

where $\Delta H_m$ is the heat of fusion per gram of copolymers determined based on the endothermic peak. 136.4 J/g ($\Delta H_{m,0}$) was used as a reference for the melting enthalpy of 100% crystalline PCL.[42] $W_{PCL}$ is the weight fraction of PCL in the copolymer which was calculated by $^1$H NMR integral areas.

**Thermal Gravimetric Analysis (TGA).** TGA was performed on a Discovery TGA from TA Instruments under a nitrogen flow rate of 100 mL/min. The sample was heated to 800 °C, and the heating rate was set at 10 °C/min.

**Dynamic Light Scattering (DLS).** A commercial LLS spectrometer (ALV/DLS/SLS-5022F) equipped with a multi-$\tau$ digital time correlator (ALV5000) was used. The Laplace inversion of each measured intensity−intensity time correlation function $G^{(2)}(q,t)$ in the self-beating mode using both the cumulants and CONTIN analysis can result in a line-width distribution $G(\Gamma)$. Then $G(\Gamma)$ can be converted to translational diffusion coefficient distribution $G(D)$ according to the equation $\Gamma = Dq^2$. The hydrodynamic radius distribution $f(R_h)$ can be obtained via the Stokes−Einstein equation, $R_h = k_BT/6\pi\eta_0 D$, where $k_B$, $T$, and $\eta_0$ are the Boltzmann constant, the absolute temperature, and the viscosity of solvent, respectively. The scattering angle was fixed at 30°, and the temperature was controlled at 25 °C. The concentration for all the samples was fixed at 0.6 mg/mL. In a typical degradation process, the oxygen in SAs solution (2 mL) was removed by bubbling nitrogen for 10 min, and then 3.2 mg of DTT was added into the solution. All the solutions were filtered through hydrophilic filters (Millipore, aperture 0.45 $\mu$m) before DLS measurements.

**Cell Viability Assay.** HeLa cells were seeded in 96-well plates (4 × $10^3$ cells per well) with 100 $\mu$L complete Dulbecco's Modified Eagle Medium (DMEM) per well and cultured for 24 h. The cells were incubated with predetermined amounts of bare polymeric SAs or DOX-loaded SAs at 37 °C and 5% $CO_2$ for 48 h. Then, 20 $\mu$L of 5 mg/mL MTT solution in phosphate buffered saline (PBS) was added to each well and incubated for another 4 h. The medium was removed carefully, and generated MTT−formazan was dissolved in 200 $\mu$L of DMSO per well. The absorbance was measured on a Bio-Rad iMark at a wavelength of 595 nm. The relative cell viability (%) was determined by comparing the absorbance at 595 nm with control wells incubated with complete DMEM. Data are presented as mean ± standard deviation (SD) ($n$ = 4).

**CMC Measurement.** The critical micelle concentration (cmc) was determined using pyrene as a fluorescence probe.[43] The fluorescence excitation spectra of pyrene were recorded by a Hitachi F-4600 fluorescence spectrophotometer (Hitachi High-Technologies Corporation, Tokyo, Japan). The emission wavelength was set at 390 nm. The concentration of polymers varied from 1.0 × $10^{-5}$ to 0.6 mg/mL, and the concentration of pyrene was fixed at 8.0 × $10^{-7}$ mol/L. The cmc was estimated as the cross-point when extrapolating the intensity ratio $I_{338}/I_{335}$ at low and high concentration regions (Figure S2).

## RESULTS AND DISCUSSION

**Synthesis and Characterization of Hyperblock and Hypergraft Copolymers.** In this study, to investigate the effect of chain architecture, two amphiphilic hyperbranched polymers (AHPs) with a similar weight fraction of hydrophobic/hydrophilic composition but different block distributions were prepared; to study the effect of block composition, the block length was systematically varied for a given hyperbranched structure. The biocompatible poly(ε-caprolactone) (PCL) was used as hydrophobic building block. We chose poly[tri(ethylene glycol) methyl ether acrylate] (PTEGMA) as hydrophilic building block because the polymerization process is well controlled and the end group can be easily modified. Scheme 2 shows our strategy of synthesizing $AB_2$-type macromonomers and the target Hyperblock and Hypergraft copolymers. The Hyperblock (HB-PCL-*b*-PTEGMA) is made from PCL-*b*-PTEGMA diblock $AB_2$-type macromonomer, and the inserted PCL and PTEGMA blocks are randomly distributed along the backbones, while the Hypergraft (HB-PCL-*g*-PTEGMA) is composed of a hyperbranched PCL core and grafted PTEGMA chains on periphery.

The synthesis started from two functional initiators, as shown in Scheme 2. The initiators I (Figure S3) and II were prepared according to our previous protocols.[35] For the synthesis of Hyperblock HB-PCL-*b*-PTEGMA and Hypergraft HB-PCL-*g*-PTEGMA, two kinds of functional $AB_2$-type macromonomers were prepared, namely, PCL-*b*-PTEGMA-$2N_3$ (Scheme 2a) and PCL-$2N_3$ (Scheme 2b). For the synthesis of PCL-*b*-PTEGMA-$2N_3$, the diblock precursor PCL-*b*-PTEGMA-OH-Br was first prepared by a combination of ring-opening polymerization (ROP) of CL and subsequent atom transfer radical polymerization (ATRP) of TEGMA. Further functional modification of the end hydroxyl group of PCL block and azidation substitution furnished the diblock macromonomer PCL-*b*-PTEGMA-$2N_3$ with one alkyne group in middle of two blocks and two azide groups located at the end of each block. The synthesis of PCL-$2N_3$ is much simpler; namely, a combination of ROP of CL, functional modification, and azidation substitution results in the final PCL-$2N_3$ macromonomer with one alkyne group in the chain center and two azide groups located at the two chain ends.

In the syntheses, the ROP and ATRP polymerization processes were all conducted in a living manner. The successful preparation of macromonomers PCL-*b*-PTEGMA-$2N_3$ and PCL-$2N_3$ with different chain lengths and block compositions was confirmed by various characterization methods. Namely, Figure 1 demonstrates that the resultant macromonomers

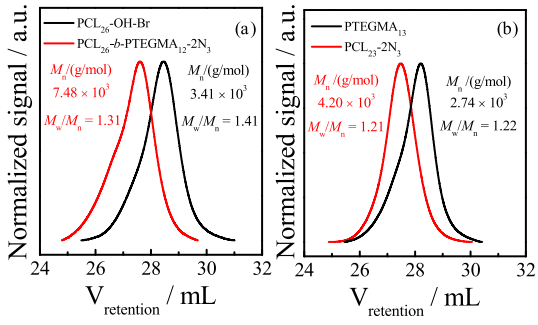


**Figure 1.** GPC curves of (a) $PCL_{26}$-OH-Br and $PCL_{26}$-*b*-$PTEGMA_{12}$-$2N_3$ and (b) $PTEGMA_{13}$ and $PCL_{23}$-$2N_3$.

$PCL_{26}$-*b*-$PTEGMA_{12}$-$2N_3$ and $PCL_{23}$-$2N_3$ own relatively narrow molar mass distributions with polydispersity indexes ($M_w/M_n$) of ∼1.3 and ∼1.2, respectively. It is worth noting that the monomer conversion during polymerization was maintained below 60% to ensure high end-group functionality. The number-average molar masses ($M_n$) were determined to be ∼7.5 × $10^3$ and ∼4.2 × $10^3$ g/mol for these two macromonomers.



DOI: 10.1021/acs.macromol.8b01784
Macromolecules 2019, 52, 1173−1187

In addition to the visual GPC measurements, the two macromonomers and other intermediate polymers were also characterized by $^1$H NMR in detail. Figures 2 and 3 summarize

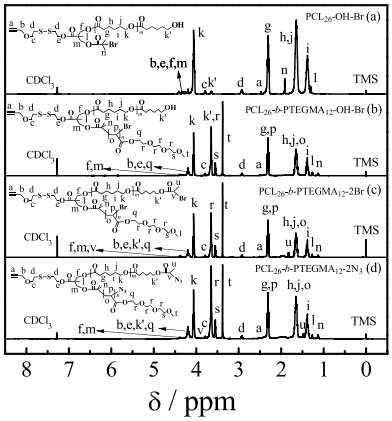


**Figure 2.** $^1$H NMR spectra of (a) $PCL_{26}$-OH-Br, (b) $PCL_{26}$-*b*-$PTEGMA_{12}$-OH-Br, (c) $PCL_{26}$-*b*-$PTEGMA_{12}$-2Br, and (d) macromonomer $PCL_{26}$-*b*-$PTEGMA_{12}$-$2N_3$.

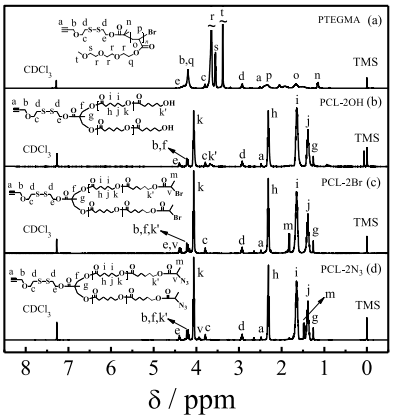


**Figure 3.** $^1$H NMR spectra of (a) $PTEGMA_{13}$, (b) $PCL_{23}$-2OH, (c) $PCL_{23}$-2Br, and (d) macromonomer $PCL_{23}$-$2N_3$.

the corresponding $^1$H NMR results for $PCL_{26}$-*b*-$PTEGMA_{12}$-$2N_3$ and $PCL_{23}$-$2N_3$, respectively. The successful polymerization and postpolymerization modification can be clearly reflected in the presence of new peaks and obvious signal shift of existing peaks, respectively. Detailed notation is made to assign the peaks to the corresponding protons of each intermediate polymer. Figure 2a shows that the characteristic peaks located at ∼4.00 ppm ("k") and ∼3.65 ppm ("k′") are attributed to the protons of $-CH_2OOC-$ and $-CH_2-OH$ on the chain backbone and the chain end of each PCL block, respectively. $PCL_{26}$-*b*-$PTEGMA_{12}$-OH-Br was obtained by subsequent ATRP of the monomer TEGMA. The new peaks located at ∼3.55 ppm ("s") and ∼3.38 ppm ("t") in Figure 2b are attributed to the protons of TEGMA repeating unit. After functional modifications by bromination reaction, the new peaks in Figure 2c located at 1.82 ppm ("u") and 4.35 ppm ("v") indicate the success of this reaction. After the azidation reaction of $PCL_{26}$-*b*-$PTEGMA_{12}$-2Br with $NaN_3$, we got the final amphiphilic macromonomer $PCL_{26}$-*b*-$PTEGMA_{12}$-$2N_3$. The $^1$H NMR spectrum is shown in Figure 2d. The peaks "u" and "v" both shift to lower position compared with $PCL_{26}$-*b*-$PTEGMA_{12}$-2Br. Moreover, the similar chemical shift changes after the synthesis process of $PCL_{23}$-$2N_3$ are shown in Figure 3. Note that GPC result can only provide apparent values for molar mass related information if we consider the difference of hydrodynamic sizes between PCL/PTEGMA and polystyrene calibration standards. Therefore, $^1$H NMR spectra were further used to extract the information about real molar mass and relative mass fraction of each block for macromonomers $PCL_{26}$-*b*-$PTEGMA_{12}$-$2N_3$ and $PCL_{23}$-$2N_3$. Principally, the relative intensity of integral area of the signals from initiating site, end-group, and monomer units can be used to calculate the real degree of polymerization (DP) for PCL and PTEGMA blocks. The value of DP of PCL segment was calculated as

$$DP_{PCL} = (A_k + A_{k'})/A_{k'} \quad (4)$$

where $A_k$ and $A_{k'}$ represent the integration area of peaks $k$ and $k'$, respectively. Similarly, the values of DP of PTEGMA block and macromonomer PCL-$2N_3$ can be calculated as

$$DP_{PTEGMA} = 2A_s/A_d \quad (5)$$

$$DP_{PCL} = 2(A_k + A_{k,})/A_{k'} \quad (6)$$

Following this principle, for $PCL_{26}$-*b*-$PTEGMA_{12}$-$2N_3$, the real DP value of PCL and PTEGMA blocks was found to be ∼26 and ∼12, respectively, while the DP value of PCL was found to be ∼23 for $PCL_{23}$-$2N_3$. In addition, the alkyne-functional PTEGMA with different lengths prepared by ATRP was further used as grafting chains for the preparation of Hypergraft HB-PCL-*g*-PTEGMA. By taking $PTEGMA_{13}$ as an example, the $^1$H NMR result demonstrates that the DP value for $PTEGMA_{13}$ is ∼13, which is similar to the PTEGMA block in the diblock copolymer $PCL_{26}$-*b*-$PTEGMA_{12}$. The corresponding GPC and $^1$H NMR curves of $PTEGMA_{13}$ are shown in Figures 1b and 3a.

The interchain coupling of macromonomer $PCL_{26}$-*b*-$PTEGMA_{12}$-$2N_3$ was conducted with the CuBr/PMDETA catalyst system to produce Hyperblock HB-$PCL_{26}$-*b*-$PTEGMA_{12}$. Similarly, the hydrophobic hyperbranched core of Hypergraft HB-$PCL_{23}$-*g*-$PTEGMA_{13}$ was prepared from macromonomer $PCL_{23}$-$2N_3$. Figure 4 shows clear shifts of

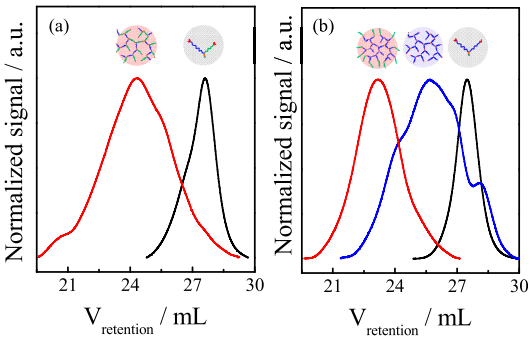


**Figure 4.** GPC curves of (a) unfractionated Hyperblock HB-$PCL_{26}$-*b*-$PTEGMA_{12}$ and macromonomer $PCL_{26}$-*b*-$PTEGMA_{12}$-$2N_3$ and (b) fractionated Hypergraft HB-$PCL_{23}$-*g*-$PTEGMA_{13}$, HB-$PCL_{23}$, and $PCL_{23}$-$2N_3$.

elution peaks in GPC curves for macromonomers $PCL_{26}$-*b*-$PTEGMA_{12}$-$2N_3$ and $PCL_{23}$-$2N_3$ after click reaction (red curves), signifying the formation of hyperbranched chains. For the preparation of Hypergraft HB-$PCL_{23}$-*g*-$PTEGMA_{13}$, an additional click reaction between the alkyne group of $PTEGMA_{13}$ and residual azide groups of PCL hyperbranched


DOI: 10.1021/acs.macromol.8b01784
Macromolecules 2019, 52, 1173−1187

core was carried out to couple the hydrophilic PTEGMA onto the periphery of PCL hyperbranched core. The GPC curve further shifts to a lower retention time, indicating the successful grafting process. All the apparent molar mass information about related samples is summarized in Table S1.

Figure 5 shows the $^1$H NMR spectra of two hyperbranched model systems. As shown, the observed new peak located at

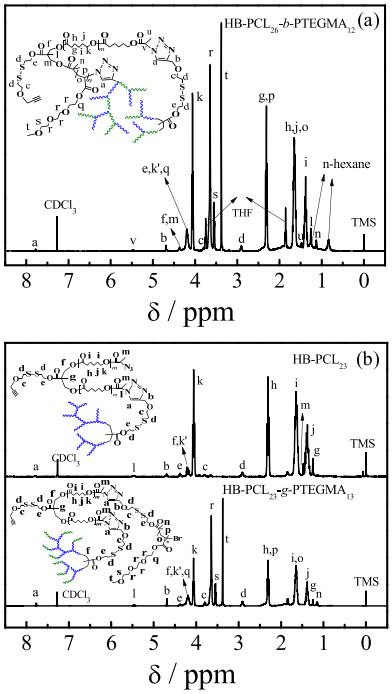


**Figure 5.** $^1$H NMR spectra of (a) Hyperblock HB-PCL$_{26}$-*b*-PTEGMA$_{12}$ and (b) hyperbranched core HB-PCL$_{23}$ and Hypergraft HB-PCL$_{23}$-*g*-PTEGMA$_{13}$.

~7.8 ppm ("a") can be attributed to the proton signal from the triazole ring,[44] indicating the formation of a triazole five-membered ring, which is also reflected in the significant chemical shifts of protons "b" and "v" from the branching linkages and terminal groups of macromonomers. Figure S4 further shows the FTIR spectra of macromonomers, hyperbranched polymers, and other intermediate polymers. Obviously, the strong vibration at ~2100 cm$^{-1}$ can be ascribed to azide asymmetric stretching vibration,[35,44] reflecting the successful substitution of bromine groups by azide groups for macromonomers PCL$_{26}$-*b*-PTEGMA$_{12}$-2N$_3$ and PCL$_{23}$-2N$_3$. After the click reaction, the vibration intensity decreases, reflecting the decrease in the mass fraction of azide groups during polycondensation process. The significant difference between final Hyperblock HB-PCL$_{26}$-*b*-PTEGMA$_{12}$ and Hypergraft HB-PCL$_{23}$-*g*-PTEGMA$_{13}$ is indicated by the stretching vibration intensity of azide groups. The vibration signal of azide groups of HB-PCL$_{23}$-*g*-PTEGMA$_{13}$ seems to totally disappear after the grafting process, indicating the high grafting efficiency (up to 90%). Overall, the structures of resultant Hyperblock HB-PCL$_{26}$-*b*-PTEGMA$_{12}$ and Hypergraft HB-PCL$_{23}$-*g*-PTEGMA$_{13}$ amphiphilic copolymers were confirmed by a combination of GPC, $^1$H NMR, and FTIR characterization. The above results clearly demonstrate that the two model hyperbranched systems have a similar PCL/PTEGMA composition but different block sequences and distributions, which can be further used as meaningful reference models for the investigation of how the block sequence and distribution affect the degradation behavior.

For HB-PCL-*b*-PTEGMA, we systematically regulated the chain length of the hydrophilic PTEGMA block in the macromonomer to obtain a set of HB-PCL$_x$-*b*-PTEGMA$_y$ with almost identical hydrophobic block ($x$ = 25−26) but with different PTEGMA block lengths ($y$ = 6, 12, and 26). For HB-PCL$_{x'}$-*g*-PTEGMA$_{y'}$, we also got a set of samples with identical hydrophobic block ($x'$ = 23−25) but with different PTEGMA block lengths ($y'$ = 12 and 21). The detailed GPC characterization results of these samples are shown in Figure S5 ($^1$H NMR and FTIR results are not shown), and their chain parameters are summarized in Table S3.

**Degradation of Hyperblock and Hypergraft Copolymers in an Organic Solvent.** As mentioned earlier, each branching point of HB-PCL-*b*-PTEGMA and HB-PCL-*g*-PTEGMA contains only one cleavable disulfide bond. All the degradable sites are perfectly distributed along the hyperbranched backbone. Following our previous study of degradable hyperbranched polystyrene, we preferred to choose dithiothreitol (DTT)[45] as the reducing agent because (1) its induced disulfide reduction is highly efficient because of its high conformational tendency to form a six-membered ring and (2) it is soluble in a range of solvents such as THF and water, providing an opportunity to carry out the experiments in both nonaqueous and aqueous solutions.

Hyperblock HB-PCL$_{26}$-*b*-PTEGMA$_{12}$ and Hypergraft HB-PCL$_{23}$-*g*-PTEGMA$_{13}$ were used as model samples to investigate the degradation behavior of hyperbranched copolymers in organic solvent. In experiments, the degradation of model samples in THF solution (10 mM DTT) was monitored quantitatively by GPC. As shown in Figures 6a and

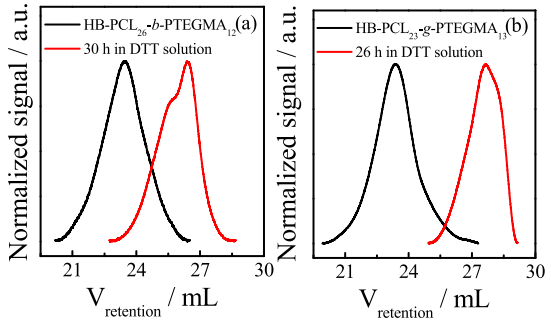


**Figure 6.** GPC curves for the two AHPs before and after degradation in THF at [DTT] = 10 mM: (a) fractionated HB-PCL$_{26}$-*b*-PTEGMA$_{12}$ and (b) fractionated HB-PCL$_{23}$-*g*-PTEGMA$_{13}$.

6b (data for reference samples are shown in Figure S6), the degradation of HB-PCL$_{26}$-*b*-PTEGMA$_{12}$ and HB-PCL$_{23}$-*g*-PTEGMA$_{13}$ is almost accomplished within ~30 h.[46] The apparent molecular information about the degradation products is summarized in Table S2. However, the nonaqueous solution is not the appropriate choice to mimic the real environment of drug releasing process. Taking the advantages of biocompatibility and water solubility of prepared Hyperblock HB-PCL-*b*-PTEGMA and Hypergraft HB-PCL-*g*-PTEGMA, we further monitored the degradation behavior of their self-assembly amphiphiles (SAs) in aqueous solutions (10 mM DTT) by stand-alone laser light scattering (LLS). The changes in the relative scattering intensity ($I_t/I_0$) and hydrodynamic radius ($\langle R_h \rangle$) were monitored over degradation time.



DOI: 10.1021/acs.macromol.8b01784
Macromolecules 2019, 52, 1173−1187

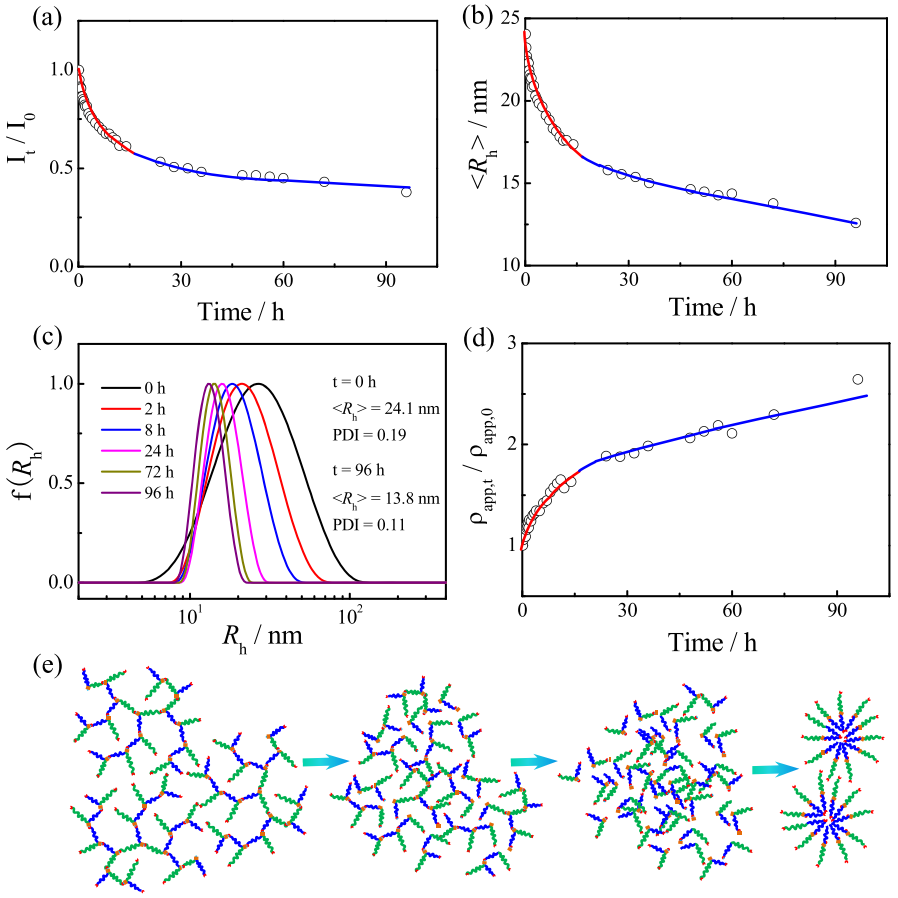


**Figure 7.** Degradation time ($t$) dependence of (a) ratio ($I_t/I_0$) of scattering intensities at $t = t$ ($I_t$) and $t = 0$ ($I_0$), (b) average hydrodynamic radius $\langle R_h \rangle$, (c) hydrodynamic radius distribution $f(R_h)$, and (d) ratio ($\rho_{app,t}/\rho_{app,0}$) of apparent chain segment densities at $t = t$ ($\rho_{app,t}$) and $t = 0$ ($\rho_{app,0}$) for HB-PCL$_{26}$-*b*-PTEGMA$_{12}$ SAs in aqueous solutions with [DTT] = 10 mM, where $C_{polymer}$ = 0.6 mg/mL. (e) Schematic illustration of degradation process for HB-PCL-*b*-PTEGMA SAs in aqueous solution.

**Degradation of Hyperblock and Hypergraft Copolymers in Aqueous Solutions: The Effect of Chain Architecture.** Using HB-PCL$_{26}$-*b*-PTEGMA$_{12}$ and HB-PCL$_{23}$-*g*-PTEGMA$_{13}$ with a similar block composition as model samples, we first investigated how the block distribution influences the degradation behavior of hyperbranched SAs in aqueous solutions. The results of degradation study for HB-PCL$_{26}$-*b*-PTEGMA$_{12}$ SAs are summarized in Figure 7. Figure 7a shows that the relative scattering intensity $I_t/I_0$ decreases rapidly in the first 20 h and then smoothly with degradation time, signifying a two-step degradation process (red and blue lines). The two-step degradation process can also be reflected in the evolution of $\langle R_h \rangle$ as a function of degradation time in Figure 7b, where the $\langle R_h \rangle$ of HB-PCL$_{26}$-*b*-PTEGMA$_{12}$ SAs rapidly decreases from ∼24 to ∼17 nm within the first 20 h, and subsequently a smooth decrease to ∼12 nm can be observed in the following 80 h. Moreover, Figure 7c shows that the hydrodynamic radius distribution $f(R_h)$ becomes narrower as time proceeds, signifying the uniformity of the SAs composed of degradation products. It is worth noting that we also measured the $f(R_h)$ of SAs composed of diblock PCL$_{26}$-*b*-PTEGMA$_{12}$ macromonomer in aqueous solution for comparison (Figure S7), which shows similar $\langle R_h \rangle$s and polydispersity indexes to those of degradation products, implying that the molecular structure of degradation products is similar to that of the macromonomer.

Figure 7d further shows that the relative apparent chain density ($\rho_{app,t}/\rho_{app,0}$), defined as $\rho_{app,t}/\rho_{app,0} = (I_t/\langle R_h \rangle^3)_{t=t}/(I_t/\langle R_h \rangle^3)_{t=0}$, gradually increases with the degradation time. This change reflects that the SAs made of huge hyperbranched chains own a much lower apparent chain density than that of initial linear macromonomer, which can be attributed to the more compact structure of SAs composed of diblock amphiphiles. By taking $R_h \sim M^{0.5}$ into $\rho \sim M/R_h^3$ for hyperbranched chains in a good solvent,[47] we can get $\rho \sim M^{-0.5}$; i.e., a polymer chain with a smaller molecular weight has a higher apparent chain density. Thus, the apparent chain density increases with the degradation of Hyperblock copolymers. It is also worth noting that the intermediate and final degradation product (PCL$_{26}$-*b*-PTEGMA$_{12}$) is not able to be further cleaved into individual PCL and PTEGMA blocks as they are chemically bonded, which leads to an unchanged hydrophobic/hydrophilic balance for SAs during the whole degradation process. At any point, no turbidity was observed in the SAs aqueous solution, even at the end of experiment. The degradation process for Hyperblock HB-PCL$_{26}$-*b*-PTEGMA$_{12}$ is schematically illustrated in Figure 7e.

In contrast, HB-PCL$_{23}$-*g*-PTEGMA$_{13}$ SAs showed different degradation kinetics as shown in Figures 8a−d. We hypothesize that this difference originates from the different branching patterns of the two model systems; namely, the PCL/PTEGMA blocks are randomly distributed within the whole framework of Hyperblock HB-PCL-*b*-PTEGMA, while


DOI: 10.1021/acs.macromol.8b01784
*Macromolecules* 2019, 52, 1173−1187

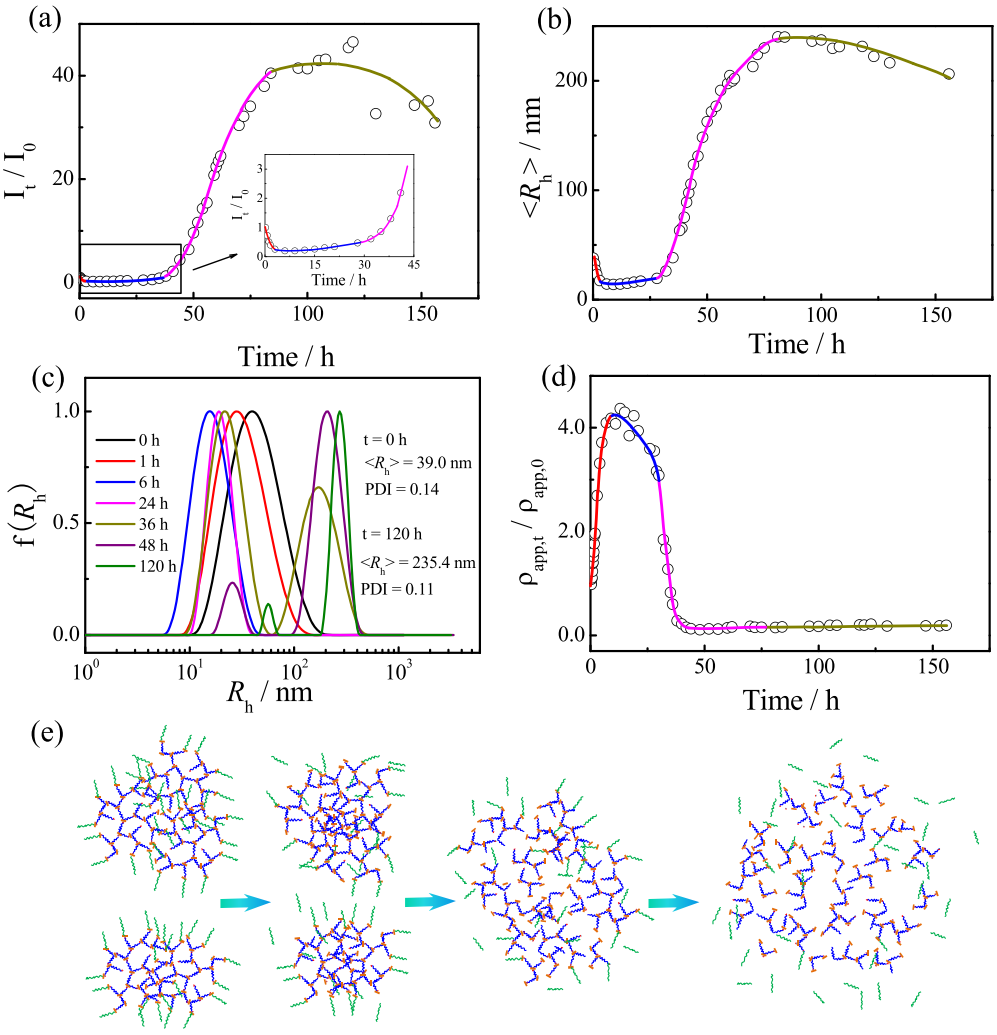


**Figure 8.** Degradation time ($t$) dependence of (a) ratio ($I_t/I_0$) of scattering intensities $t = t$ ($I_t$) and $t = 0$ ($I_0$), (b) average hydrodynamic radius $\langle R_h \rangle$, (c) hydrodynamic radius distribution $f(R_h)$, and (d) ratio ($\rho_{app,t}/\rho_{app,0}$) of apparent chain segment densities at $t = t$ ($\rho_{app,t}$) and $t = 0$ ($\rho_{app,0}$) for HB-PCL$_{23}$-*g*-PTEGMA$_{13}$ SAs in aqueous solutions with [DTT] = 10 mM, where $C_{polymer}$ = 0.6 mg/mL. (e) Schematic illustration of degradation process for HB-PCL-*g*-PTEGMA SAs in aqueous solution.

spatially separated hydrophobic PCL and hydrophilic PTEGMA domains exist for Hypergraft HB-PCL-*g*-PTEGMA. Relying on the observed different change rates in light scattering intensity and size, the whole degradation process can be divided into four time intervals: (i) $t$ < 4 h, a fast degradation process was observed, reflected in the significant decrease of $I_t/I_0$ from ~1.0 to ~0.3 (Figure 8a) and size from ~24 to ~16 nm (Figures 8b,c); (ii) 4 h < $t$ < 29 h, the determined values of $I_t/I_0$ and $\langle R_h \rangle$ weakly increase with time; (iii) 29 h < $t$ < 82 h, $I_t/I_0$ and $\langle R_h \rangle$ start to rapidly increase with degradation time, ~12 times increase in $\langle R_h \rangle$ was observed; (iv) $t$ > 82 h, the average size of assemblies slowly decreases with degradation time.

Reasonably, the change during the first time interval could be mainly attributed to the degradation process of the PTEGMA shell, where the DTT molecules can quickly permeate the periphery of Hypergraft HB-PCL$_{23}$-*g*-PTEGMA$_{13}$ due to the hydrophilic nature of PTEGMA shells. The phenomenon of second time interval can be related to the balance between degradation and aggregation of SAs. As mentioned earlier, the hydrophobic/hydrophilic balance is almost constant for Hyperblock HB-PCL$_{26}$-*b*-PTEGMA$_{12}$ during the degradation process, while this is not the case for Hypergraft HB-PCL$_{23}$-*g*-PTEGMA$_{13}$. As shown in Figure 8e, there is always one disulfide linkage between PCL and PTEGMA blocks, which leads to the fact that both the PCL and PTEGMA blocks in hyperbranched assemblies can be independently degraded, inevitably leading to significant change in hydrophobic/hydrophilic balance of remaining assemblies. Consequently, the weight fraction of hydrophobic PCL blocks on some of Hypergraft chains and their assemblies will significantly increase as the degradation proceeds, resulting in the disturbance of the hydrophobic/hydrophilic balance. Thermodynamically, aggregation of unstable SAs with high content of PCL blocks inevitably leads to an increase in both apparent molar mass and hydrodynamic radius of SAs.

Furthermore, it is not difficult to understand the experimental phenomenon in the third time interval between 29 h < $t$ < 82 h, where the cleavage of disulfide bonds further leads to serious imbalance of hydrophobicity/hydrophilicity and strong aggregation of degradation products. It is resonable to predict that the aggregation process will finally determine the apparent molar mass and size of SAs existing in the system. Indeed, macroscopic precipitates were observed at the bottom


DOI: 10.1021/acs.macromol.8b01784
*Macromolecules* 2019, 52, 1173−1187

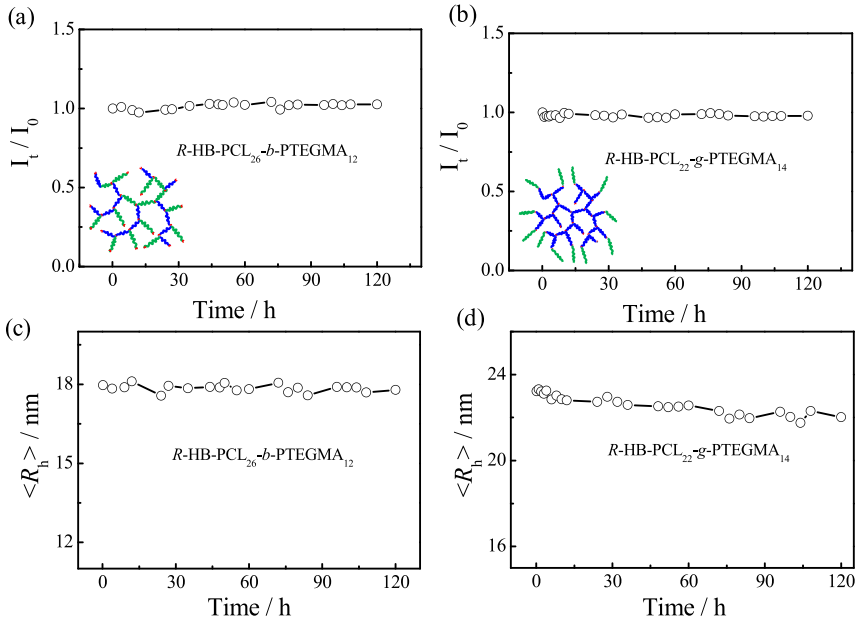


**Figure 9.** Degradation time ($t$) dependence of (a) and (b) ratio ($I_t/I_0$) of scattering intensities at $t = t$ ($I_t$) and $t = 0$ ($I_0$); (c) and (d) average hydrodynamic radius $\langle R_h \rangle$ for *R*-HB-PCL$_{26}$-*b*-PTEGMA$_{12}$ and *R*-HB-PCL$_{22}$-*g*-PTEGMA$_{14}$ SAs in aqueous solutions with [DTT] = 10 mM.

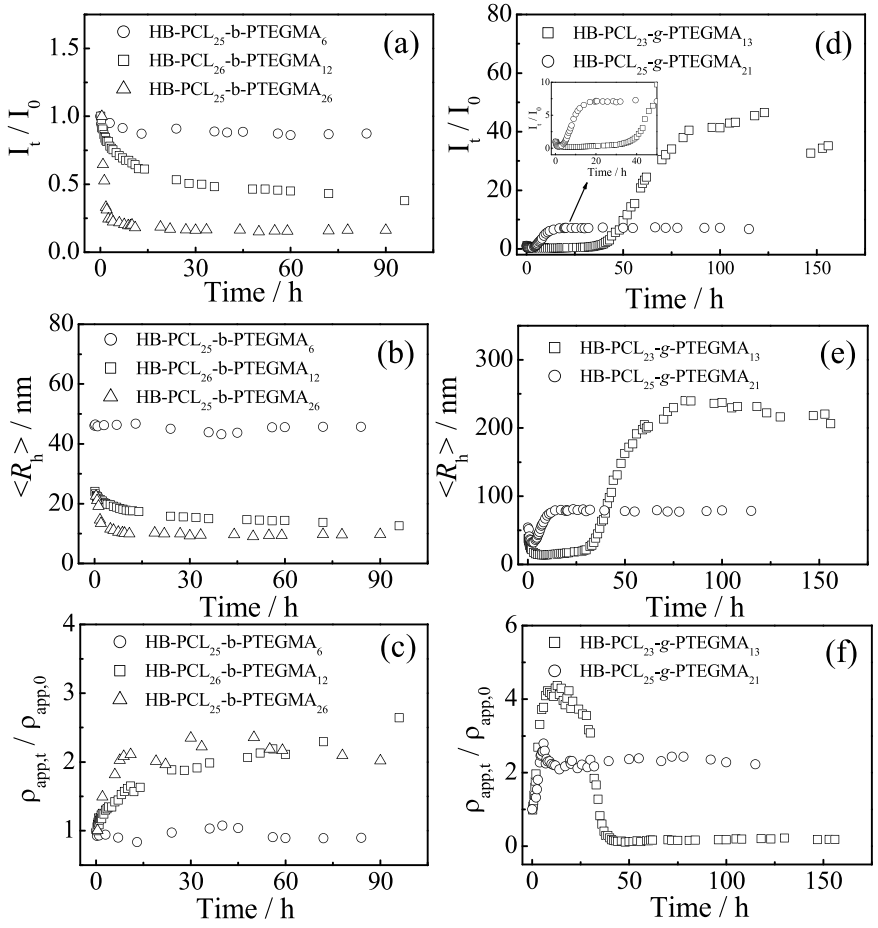


**Figure 10.** Degradation time ($t$) dependence of (a, d) ratio ($I_t/I_0$) of scattering intensities at $t = t$ ($I_t$) and $t = 0$ ($I_0$); (b), (e) average hydrodynamic radius $\langle R_h \rangle$; (c, f) ratio ($\rho_{app,t}/\rho_{app,0}$) of chain segment densities at $t = t$ ($\rho_{app,t}$) and $t = 0$ ($\rho_{app,0}$) for SAs of HB-PCL-*b*-PTEGMA and HB-PCL-*g*-PTEGMA with different compositions in aqueous solutions with [DTT] = 10 mM, where $C_{polymer}$ = 0.6 mg/mL.

of experimental vial after 100 h, further supporting our explanation.

The changes in apparent chain density can be interpreted as follows: (1) For the first time interval, the degradation of



DOI: 10.1021/acs.macromol.8b01784
*Macromolecules* 2019, 52, 1173−1187

PTEGMA shell leads to a compact structure. Thus, the apparent chain density increases. (2) For the second time interval, both of the disulfide linkages in the shell and core degrade. However, the degradation of disulfide linkages in the hydrophobic core leads to a loose structure. The combination effect shows a little decrease in the apparent chain density. (3) For the third and the fourth time intervals, more and more disulfide linkages were degraded. Large but loose aggregates were generated, so the $M$ increased and the apparent chain density decreased as $\rho \sim M^{-0.5}$. Moreover, it should be noted that for the fourth time interval the measured chain apparent density is related to the species suspended in the solutions due to the formation of precipitates.

The TEM data (Figures S8 and S9) also show similar evolution during the course of degradation in an aqueous phase. On the basis of the above results, it is clear that even for hyperbranched systems with a similar block composition, the difference of the sequence and spatial distribution of hydrophobic/hydrophilic blocks can also lead to distinct degradation behavior of hyperbranched assemblies. The above results also highlight the importance of utilizing model samples with controlled branching structure and degradable sites for the structure−property study. Overall, the Hypergraft HB-PCL-*g*-PTEGMA presented a much more complicated degradation process.

Up until now, the result has shown how the branching pattern of amphiphilic hyperbranched assemblies affects their degradation in aqueous solutions and quantitatively analyzed the chain architecture−degradation property relation. However, for unambiguous conclusion, the reference hyperbranched systems without cleavable disulfide bonds should also be studied for meaningful comparison. Thus, we further prepared two reference samples without disulfide linkages named *R*-HB-$PCL_{26}$-*b*-$PTEGMA_{12}$ and *R*-HB-$PCL_{22}$-*g*-$PTEGMA_{14}$ for control experiments. The $^1$H NMR, FTIR, and GPC measurements confirmed the structures of the initiators, macromonomers, and resultant hyperbranched polymers (Figures S10−S16), and the synthesis details can be found in Schemes S1 and S2.

Overall, compared with HB-$PCL_{26}$-*b*-$PTEGMA_{12}$ and HB-$PCL_{23}$-*g*-$PTEGMA_{13}$, the two reference samples own a similar composition of hydrophobic/hydrophilic block and overall average molar mass (Figure S15). Moreover, the size of SAs composed of the two reference AHPs is determined to be ∼18 and ∼23 nm, respectively, very close to the previously measured sizes for HB-$PCL_{26}$-*b*-$PTEGMA_{12}$ and HB-$PCL_{23}$-*g*-$PTEGMA_{13}$, demonstrating that the existing disulfide linkages on the branching units actually play negligible role in affecting the hydrophobic/hydrophilic balance. More importantly, the LLS study of degradation kinetics of the two reference AHPs shows no evidence for their degradation in aqueous solutions, reflected by the constant scattering intensity and average hydrodynamic size (Figure 9), further proving that the observed decrease of light scattering intensity and average hydrodynamic size is indeed originated from the cleavage of disulfide bonds instead of the degradation of PCL block.

**Degradation of Hyperblock and Hypergraft Copolymers in Aqueous Solutions: The Effect of Block Composition.** For a given chain architecture, the block composition is also important for the regulation of degradation behavior of resultant hyperbranched amphiphiles. Thus, we studied how the hydrophilic block length affects the self-assembly and degradation of Hyperblock and Hypergraft copolymers. As shown in Figures 10a,b for Hyperblock HB-$PCL_x$-*b*-$PTEGMA_y$, as the DP of PTEGMA increases from 6 to 26, the degradation rate significantly increases, reflected in the evolutions of $I_t/I_0$ and $\langle R_h \rangle$ with degradation time. Specifically, no obvious change was observed for HB-$PCL_{25}$-*b*-$PTEGMA_6$ with shortest PTEGMA block length, and we attributed this phenomenon to frozen state of the amphiphilic SAs induced by the strong hydrophobic interaction between $PCL_{25}$ blocks. Namely, even the cleavable disulfide bonds could be attacked by DTT molecules; the diffusion of degradation product $PCL_{25}$-*b*-$PTEGMA_6$ might be completely prohibited due to the much strong hydrophobic interaction among $PCL_{25}$ blocks in $PCL_{25}$-*b*-$PTEGMA_6$. Figure 10c quantitatively shows that the apparent density monotonically increases with degradation time for HB-$PCL_{26}$-*b*-$PTEGMA_{12}$ and HB-$PCL_{25}$-*b*-$PTEGMA_{26}$.

Figures 10d−f summarize the corresponding results for Hypergraft copolymers HB-$PCL_{x'}$-*g*-$PTEGMA_{y'}$. Clearly, a four-step degradation process was also observed for HB-$PCL_{25}$-*g*-$PTEGMA_{21}$ with longer PTEGMA block length. For HB-$PCL_{25}$-*g*-$PTEGMA_{21}$, the transition points of the degradation curve shift to earlier time points, reflecting the accelerated degradation process, but the number of transition points is unchanged as the PTEGMA block length increases, indicating that the structures for SAs with different PTEGMA block lengths are almost similar.

The above studies unambiguously reveal that the factors of chain architecture and block composition play different roles for the regulation of degradation behavior of long-subchain hyperbranched SAs; namely, the degradation model is mainly affected by the chain architecture and the structure of resultant SAs, while for a given architecture, the degradation rate can be regulated by systematically varying the block composition. Overall, the above result also demonstrates that the synergistic effect of the two factors determine the details of degradation behavior of hyperbranched SAs.

**Thermal Properties of Hyperblock and Hypergraft Copolymers in Bulk.** Another important factor that may be closely related to the degradation behavior of hyperbranched assemblies is the crystallization of the PCL block. It is known that PCL is a semicrystalline polymer; thus, its crystallization property actually plays an important role in determining both permeability and biodegradability of bulk materials,[48,49] which may further influence the degradation behavior of PCL-based assemblies in aqueous solutions. To clarify whether it is the block sequence and distribution or the crystallization of PCL block that induces the difference in observed degradation behavior of the two model systems, DSC measurements were conducted to investigate the crystallization property of these powder samples. Figure 11 shows the obtained DSC curves during reheating. The degree of crystallinity ($\chi_c$) of Hyperblock HB-$PCL_{26}$-*b*-$PTEGMA_{12}$ decreases from 41.6% to 30.4% compared with its macromonomer, indicating that the crystallization of PCL segments is suppressed by the branching structure, to some extent. However, the observed phenomenon is different from our previous work[35] for Hyperblock HB-PCL-*b*-PS, where the crystallization of PCL segments in HB-PCL-*b*-PS was completely suppressed, and no obvious crystallization behavior was observed in DSC measurement. This inconsistency can be attributed to the fact that PTEGMA block is more flexible as compared to PS block. For the Hypergraft HB-PCL-*g*-PTEGMA system shown in Figure 11b, the value of $\chi_c$


DOI: 10.1021/acs.macromol.8b01784
*Macromolecules* 2019, 52, 1173−1187

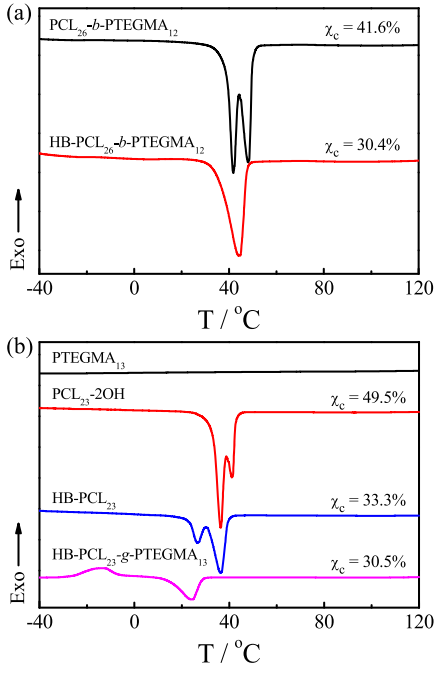


**Figure 11.** DSC curves (10 °C/min) during reheating of (a) Hyperblock HB-$PCL_{26}$-*b*-$PTEGMA_{12}$ and $PCL_{26}$-*b*-$PTEGMA_{12}$-$2N_3$. (b) Hypergraft HB-$PCL_{23}$-*g*-$PTEGMA_{13}$, $PCL_{23}$-2OH, and other intermediate polymers.

of hyperbranched PCL core is also found to be smaller than that of the macromonomer. After grafting the hydrophilic PTEGMA blocks to form the final HB-$PCL_{23}$-*g*-$PTEGMA_{13}$, the determined $\chi_c$ shows no obvious difference compared with the hyperbranched PCL core alone. The above observation further supports that as flexible segments,[50] PTEGMA blocks have little impact on the crystallization of PCL blocks. Overall, the determined degrees of crystallinity of Hyperblock HB-$PCL_{26}$-*b*-$PTEGMA_{12}$ ($\chi_c$ = 30.4%) and Hypergraft HB-$PCL_{23}$-*g*-$PTEGMA_{13}$ ($\chi_c$ = 30.5%) are almost similar to each other, further indicating that the observed difference in their degradation behavior in solution phase is unlikely to be affected by the crystallization property of the PCL block. In addition, the two reference AHPs *R*-HB-$PCL_{26}$-*b*-$PTEGMA_{12}$ and *R*-HB-$PCL_{22}$-*g*-$PTEGMA_{14}$ also show similar degrees of crystallinity (Figure S17, $\chi_c$ = 33.4% and $\chi_c$ = 32.1%), supporting the negligible influence of disulfide bonds on the crystallization of PCL.

Moreover, the TGA test was also performed for HB-$PCL_{26}$-*b*-$PTEGMA_{12}$ and HB-$PCL_{23}$-*g*-$PTEGMA_{13}$. Data are shown in Figure S18. The temperature and weight change of their decomposition reactions are almost the same. No significant differences were found between these two structures. The results may be ascribed to their similar chemical compositions.

**Studies of Drug Loading and Release.** The drug loading related properties including drug loading content (DLC) and drug loading efficiency (DLE) were also studied, where DOX was used as model hydrophobic drug. The $R_h$ values of drug loaded SAs, DLC, and DLE results are summarized in Table 1. The $R_h$ value of HB-$PCL_{23}$-*g*-$PTEGMA_{13}$-DOX is ~135 nm (Figure S19), which has a large difference with its bare SAs (~39 nm). This difference can also be seen in TEM results (Figure S20). A possible explanation for this could be ascribed to their different branching patterns of the two model systems (Scheme 3). Compared with Hyperblock SAs, the Hypergraft

**Table 1. DLC and DLE of DOX Loaded SAs**

| sample | $\langle R_h \rangle$ (nm) | DLC (%) | DLE (%) |
|---|---|---|---|
| HB-$PCL_{26}$-*b*-$PTEGMA_{12}$-DOX | 21.9 | 5.3 | 28.0 |
| HB-$PCL_{23}$-*g*-$PTEGMA_{13}$-DOX | 135.1 | 3.0 | 15.3 |

SAs own much larger and more continuous hydrophobic domains, which probably makes the assembled structures more sensitive to hydrophobic–hydrophilic balance. Consequently, the size change for Hypergraft SAs is more significant after drug loading. This difference may also induce the fact that HB-$PCL_{26}$-*b*-$PTEGMA_{12}$ possesses higher DLC and DLE than that of HB-$PCL_{23}$-*g*-$PTEGMA_{13}$. Overall, both of the systems have considerable DLC[19,22] but not that much as those reported values in previous literature.[51,52] In addition, the stability results (Figure S21) show that the average hydrodynamic radii $\langle R_h \rangle$s of drug-loaded SAs HB-$PCL_{26}$-*b*-$PTEGMA_{12}$-DOX and HB-$PCL_{23}$-*g*-$PTEGMA_{13}$-DOX remain constant within 72 h in PBS solutions with or without the addition of 10% fetal bovine serum, indicating their high stability.

In addition to the careful investigation of degradation behavior, we also performed a study of the drug release of drug-loaded SAs and the cell viability of hyperbranched assemblies with and without drug loading using HeLa cells as model cells. The drug release results indicate that Hyperblock copolymer nanostructures have a faster release rate than Hypergraft copolymer nanostructures, as shown in Figure S22. For Hyperblock copolymers, the amphiphilic blocks may release drugs in the hydrophobic domains easily once degraded from the mother structure. For Hypergraft copolymers, the hydrophobic core maintains compact structure even after some disulfide groups were degraded according to the degradation data. Figure 12a (also Figure S23) shows that without drug loading the cell viability for HB-$PCL_{26}$-*b*-$PTEGMA_{12}$ and HB-$PCL_{23}$-*g*-$PTEGMA_{13}$ SAs are >80% after 48 h incubation, indicating the biocompatibility of our hyperbranched systems. With drug loading, both of them possess good inhibition of HeLa cells proliferation. Both of them have considerable $IC_{50}$ values according to the literature,[19,53−55] and the data are shown in Figure 12b. The inhibition of HeLa cells proliferation by DOX-loaded SAs HB-$PCL_{26}$-*b*-$PTEGMA_{12}$-DOX seems better than that of the HB-$PCL_{23}$-*g*-$PTEGMA_{13}$-DOX analogue (Figure 12b) even though the HB-$PCL_{23}$-*g*-$PTEGMA_{13}$-DOX exhibits higher cell uptake than HB-$PCL_{26}$-*b*-$PTEGMA_{12}$-DOX (Figure S24). This difference can probably be attributed to their different release rates. Moreover, by comparison of the results for drug-loaded hyperbranched assemblies with and without disulfide linkages (Figure S25), the existing disulfide linkages seem to provide a better inhibition efficiency of HeLa cells proliferation due to their redox responsiveness.[56] As it is widely accepted that the intracellular glutathione (GSH) level in cancer cells is higher than that in normal cells,[57,58] the results imply that the high GSH level in cancer cells may accelerate the destabilization of SAs with disulfide linkages.[45,58,59]

## CONCLUSION

The effects of block composition and distribution on the degradation behavior of hyperbranched amphiphiles and the drug release kinetics were investigated by using a set of Hyperblock HB-PCL-*b*-PTEGMA and Hypergraft HB-PCL-*g*-PTEGMA copolymers with controlled parameters as model samples. The degradation study monitored by GPC and DLS


DOI: 10.1021/acs.macromol.8b01784
*Macromolecules* 2019, 52, 1173−1187

**Scheme 3. Schematic Illustration of Hydrophobic Domain and Loaded Drug for (a) Hyperblock HB-PCL-*b*-PTEGMA and (b) Hypergraft HB-PCL-*g*-PTEGMA**

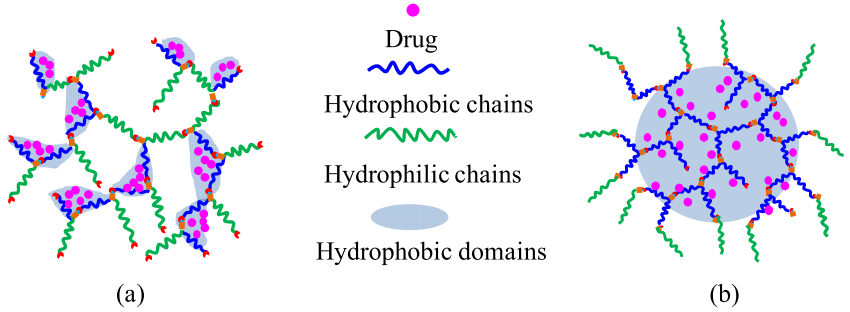


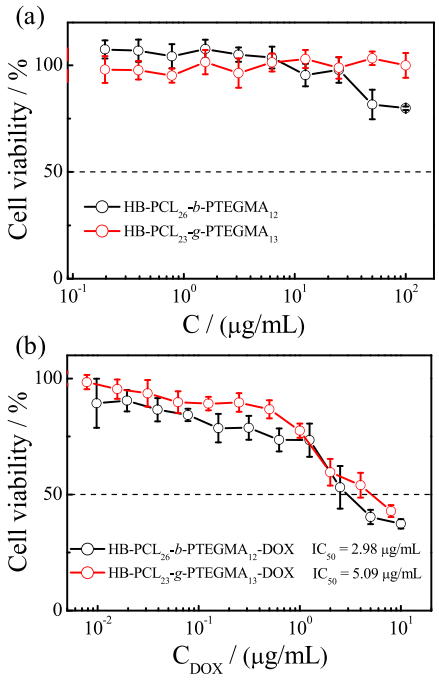


**Figure 12.** In vitro cytotoxicity of Hela cells against (a) bare polymeric SAs of Hyperblock HB-PCL$_{26}$-*b*-PTEGMA$_{12}$ and Hypergraft HB-PCL$_{23}$-*g*-PTEGMA$_{13}$ and (b) DOX loaded SAs of Hyperblock HB-PCL$_{26}$-*b*-PTEGMA$_{12}$ and Hypergraft HB-PCL$_{23}$-*g*-PTEGMA$_{13}$ for 48 h.

clearly demonstrated that both of the model systems can be degraded by using DTT as the reducing agent. In addition, the degradation results of self-assembly amphiphiles (SAs) reveal that the factors of block distribution and composition play different roles for the regulation of degradation behavior of long-subchain hyperbranched SAs; namely, the degradation process is mainly affected by the chain architecture and the structure of resultant SAs, while for a given chain architecture, the degradation rate can be regulated by systematically varying the block composition. In addition, control experiments indicated the neglected effect of embedded disulfide linkages on the crystallization of PCL block and the degradation process. It is well-known that the stability and release kinetics for a given drug-loaded SAs system will be influenced by multifactors, such as the degradation behavior of polymer assembly itself, the concentration of trigger molecules, the hydrophilic/hydrophobic balance of drug molecules, and the special interaction between drug molecules and polymer framework. It is not an easy task to realize the controlled release of target drug molecules by optimizing all these factors simultaneously. This study shows that even for hyperbranched systems with a similar hydrophobic/hydrophilic block composition, the minor change of block sequence and distribution can lead to totally different degradation behavior. Thus, a careful examination of the polymer structure–degradation property relation is the prerequisite for further comprehensive adjustment of multifactors to realize the controlled degradation of polymer assembly and release of target drug.

## ■ ASSOCIATED CONTENT

### Supporting Information

The Supporting Information is available free of charge on the ACS Publications website at DOI: 10.1021/acs.macromol.8b01784.

Molar mass information from GPC and $^1$H NMR data; schematic illustration of the synthesis of reference samples; standard curve of DOX in DMSO; fluorescence intensity ratio $I_{338}/I_{335}$; $^1$H NMR spectra; IR spectra; GPC curves; hydrodynamic radius distribution $f(R_h)$; TEM micrograph; DSC curves; TGA curves; time dependence of average hydrodynamic radius; drug release kinetics; cytotoxicity; flow cytometric analyses (PDF)

## ■ AUTHOR INFORMATION


### Corresponding Authors

*E-mail xdye@ustc.edu.cn.
*E-mail llw@mail.ustc.edu.cn.

### ORCID

Lianwei Li: 0000-0002-1996-6046
Xiaodong Ye: 0000-0003-2143-1726


### Notes

The authors declare no competing financial interest.

## ■ ACKNOWLEDGMENTS

The financial support of the National Natural Scientific Foundation of China Projects (21674107, 21774116, 51703216, and 51773192) and the Fundamental Research Funds for the Central Universities (WK2340000066) is gratefully acknowledged.

## ■ REFERENCES

(1) Wang, Y.; Grayson, S. M. Approaches for the Preparation of Non-Linear Amphiphilic Polymers and Their Applications to Drug Delivery. *Adv. Drug Delivery Rev.* **2012**, *64*, 852–865.



DOI: 10.1021/acs.macromol.8b01784
*Macromolecules* 2019, 52, 1173–1187

(2) Yates, C. R.; Hayes, W. Synthesis and Applications of Hyperbranched Polymers. *Eur. Polym. J.* **2004**, *40*, 1257−1281.
(3) Konkolewicz, D.; Gray-Weale, A.; Perrier, S. Hyperbranched Polymers by Thiol-Yne Chemistry: from Small Molecules to Functional Polymers. *J. Am. Chem. Soc.* **2009**, *131*, 18075−18077.
(4) Kurniasih, I. N.; Keilitz, J.; Haag, R. Dendritic Nanocarriers Based on Hyperbranched Polymers. *Chem. Soc. Rev.* **2015**, *44*, 4145−4164.
(5) Kim, Y. H.; Webster, O. W. Hyperbranched Polyphenylenes. *Macromolecules* **1992**, *25*, 5561−5572.
(6) Yang, G.; Jikei, M.; Kakimoto, M. A. Successful Thermal Self-Polycondensation of $AB_2$ Monomer to Form Hyperbranched Aromatic Polyamide. *Macromolecules* **1998**, *31*, 5964−5966.
(7) Stiriba, S. E.; Kautz, H.; Frey, H. Hyperbranched Molecular Nanocapsules: Comparison of the Hyperbranched Architecture with the Perfect Linear Analogue. *J. Am. Chem. Soc.* **2002**, *124*, 9698−9699.
(8) Prabaharan, M.; Grailer, J. J.; Pilla, S.; Steeber, D. A.; Gong, S. Q. Folate-Conjugated Amphiphilic Hyperbranched block Copolymers Based on Boltorn® H40, Poly(L-lactide) and Poly(ethylene glycol) for Tumor-Targeted Drug Delivery. *Biomaterials* **2009**, *30*, 3009−3019.
(9) Liu, J. Y.; Pang, Y.; Huang, W.; Zhu, X. Y.; Zhou, Y. F.; Yan, D. Y. Self-Assembly of Phospholipid-Analogous Hyperbranched Polymers Nanomicelles for Drug Delivery. *Biomaterials* **2010**, *31*, 1334−1341.
(10) Follmann, H. D.; Oliveira, O. N.; Lazarin-Bidóia, D.; Nakamura, C. V.; Huang, X.; Asefa, T.; Silva, R. Multifunctional Hybrid Aerogels: Hyperbranched Polymer-Trapped Mesoporous Silica Nanoparticles for Sustained and Prolonged Drug Release. *Nanoscale* **2018**, *10*, 1704−1715.
(11) Sideratou, Z.; Agathokleous, M.; Theodossiou, T. A.; Tsiourvas, D. Functionalized Hyperbranched Polyethylenimines as Thermosensitive Drug Delivery Nanocarriers with Controlled Transition Temperatures. *Biomacromolecules* **2018**, *19*, 315−328.
(12) Wais, U.; Chennamaneni, L. R.; Thoniyot, P.; Zhang, H.; Jackson, A. W. Main-Chain Degradable Star Polymers Composed of pH-Responsive Hyperbranched Cores and Thermoresponsive Polyethylene Glycol-Based Coronas. *Polym. Chem.* **2018**, *9*, 4824−4839.
(13) Hu, X. L.; Zhai, S. D.; Liu, G. H.; Xing, D.; Liang, H. J.; Liu, S. Y. Concurrent Drug Unplugging and Permeabilization of Polyprodrug-Gated Crosslinked Vesicles for Cancer Combination Chemotherapy. *Adv. Mater.* **2018**, *30*, 1706307.
(14) Cao, Y. W.; He, J. L.; Liu, J.; Zhang, M. Z.; Ni, P. H. Folate-Conjugated Polyphosphoester with Reversible Cross-Linkage and Reduction Sensitivity for Drug Delivery. *ACS Appl. Mater. Interfaces* **2018**, *10*, 7811−7820.
(15) Ju, P. F.; Hu, J.; Li, F.; Cao, Y. W.; Li, L.; Shi, D. J.; Hao, Y.; Zhang, M. Z.; He, J. L.; Ni, P. H. A biodegradable Polyphosphoester-Functionalized Poly (disulfide) Nanocarrier for Reduction-Triggered Intracellular Drug Delivery. *J. Mater. Chem. B* **2018**, *6*, 7263−7273.
(16) Ikladious, N. E.; Mansour, S. H.; Asaad, J. N.; Emira, H. S.; Hilt, M. Synthesis and Evaluation of New Hyperbranched Aalkyds for Coatings. *Prog. Org. Coat.* **2015**, *89*, 252−259.
(17) Grimsdale, A. C.; Leok Chan, K.; Martin, R. E.; Jokisz, P. G.; Holmes, A. B. Synthesis of Light-Emitting Conjugated Polymers for Applications in Electroluminescent Devices. *Chem. Rev.* **2009**, *109*, 897−1091.
(18) Wang, J.; Mei, J.; Zhao, E. G.; Song, Z. G.; Qin, A. J.; Sun, J. Z.; Tang, B. Z. Ethynyl-Capped Hyperbranched Conjugated Polytriazole: Click Polymerization, Clickable Modification, and Aggregation-Enhanced Emission. *Macromolecules* **2012**, *45*, 7692−7703.
(19) Liu, J. Y.; Huang, W.; Pang, Y.; Huang, P.; Zhu, X. Y.; Zhou, Y. F.; Yan, D. Y. Molecular Self-assembly of a Homopolymer: an Alternative to Fabricate Drug-delivery Platforms for Cancer Therapy. *Angew. Chem.* **2011**, *123*, 9328−9332.
(20) Lee, S.; Saito, K.; Lee, H. R.; Lee, M. J.; Shibasaki, Y.; Oishi, Y.; Kim, B. S. Hyperbranched Double Hydrophilic Block Copolymer Micelles of Poly (ethylene oxide) and Polyglycerol for pH-Responsive Drug Delivery. *Biomacromolecules* **2012**, *13*, 1190−1196.
(21) Hu, X. L.; Liu, G. H.; Li, Y.; Wang, X. R.; Liu, S. Y. Cell-Penetrating Hyperbranched Polyprodrug Amphiphiles for Synergistic Reductive Milieu-Triggered Drug Release and Enhanced Magnetic Resonance Signals. *J. Am. Chem. Soc.* **2015**, *137*, 362−368.
(22) Liu, J. Y.; Huang, W.; Pang, Y.; Zhu, X. Y.; Zhou, Y. F.; Yan, D. Y. Self-Assembled Micelles from an Amphiphilic Hyperbranched Copolymer with Polyphosphate Arms for Drug Delivery. *Langmuir* **2010**, *26*, 10585−10592.
(23) Liu, J. Y.; Pang, Y.; Huang, W.; Huang, X. Y.; Meng, L. L.; Zhu, X. Y.; Zhou, Y. F.; Yan, D. Y. Bioreducible Micelles Self-Assembled from Amphiphilic Hyperbranched Multiarm Copolymer for Glutathione-Mediated Intracellular Drug Delivery. *Biomacromolecules* **2011**, *12*, 1567−1577.
(24) Zhuang, Y. Y.; Deng, H. P.; Su, Y.; He, L.; Wang, R. B.; Tong, G. S.; He, D. N.; Zhu, X. Y. Aptamer-Functionalized and Backbone Redox-Responsive Hyperbranched Polymer for Targeted Drug Delivery in Cancer Therapy. *Biomacromolecules* **2016**, *17*, 2050−2062.
(25) Fréchet, J. M. J.; Henmi, M.; Gitsov, I.; Aoshima, S.; Leduc, M. R.; Grubbs, R. B. Self-Condensing Vinyl Polymerization: An Approach to Dendritic. *Science* **1995**, *269*, 1080−1083.
(26) Hawker, C. J.; Frechet, J. M. J.; Grubbs, R. B.; Dao, J. Preparation of Hyperbranched and Star Polymers by a "Living", Self-Condensing Free Radical Polymerization. *J. Am. Chem. Soc.* **1995**, *117*, 10763−10764.
(27) Peleshanko, S.; Gunawidjaja, R.; Petrash, S.; Tsukruk, V. V. Synthesis and Interfacial Behavior of Amphiphilic Hyperbranched Polymers: Poly(ethylene oxide)-Polystyrene Hyperbranches. *Macromolecules* **2006**, *39*, 4756−4766.
(28) Liu, M. J.; Vladimirov, N.; Fréchet, J. M. J. A New Approach to Hyperbranched Polymers by Ring-Opening Polymerization of an AB Monomer: 4-(2-Hydroxyethyl)-ε-caprolactone. *Macromolecules* **1999**, *32*, 6881−6884.
(29) Magnusson, H.; Malmström, E.; Hult, A. Synthesis of Hyperbranched Aliphatic Polyethers via Cationic Ring-Opening Polymerization of 3-ethyl-3-(hydroxymethyl)oxetane. *Macromol. Rapid Commun.* **1999**, *20*, 453−457.
(30) Hutchings, L. R.; Roberts-Bleming, S. J. DendriMacs. Well-Defined Dendritically Branched Polymers Synthesized by an Iterative Convergent Strategy Involving the Coupling Reaction of $AB_2$ Macromonomers. *Macromolecules* **2006**, *39*, 2144−2152.
(31) He, C.; Li, L. W.; He, W. D.; Jiang, W. X.; Wu, C. Click" Long Seesaw-Type A ∼ ∼B∼∼ A Chains Together into Huge Defect-Free Hyperbranched Polymer Chains with Uniform Subchains. *Macromolecules* **2011**, *44*, 6233−6236.
(32) Li, L. W.; He, C.; He, W. D.; Wu, C. Formation Kinetics and Scaling of "Defect-Free" Hyperbranched Polystyrene Chains with Uniform Subchains Prepared from Seesaw-Type Macromonomers. *Macromolecules* **2011**, *44*, 8195−8206.
(33) Li, L. W.; Zhou, J. F.; Wu, C. Intrachain Folding and Interchain Association of Hyperbranched Chains with Long Uniform Subchains Made of Amphiphilic Diblock Copolymers. *Macromolecules* **2012**, *45*, 9391−9399.
(34) Li, L. W.; He, C.; He, W. D.; Wu, C. How Does a Hyperbranched Chain Pass through a Nanopore? *Macromolecules* **2012**, *45*, 7583−7589.
(35) Yang, J. X.; Li, L. W.; Jing, Z. Y.; Ye, X. D.; Wu, C. Construction and Properties of Hyperbranched Block Copolymer with Independently Adjustable Heterosubchains. *Macromolecules* **2014**, *47*, 8437−8445.
(36) Li, L. W.; Wang, X.; Yang, J. X.; Ye, X. D.; Wu, C. Degradation Kinetics of Model Hyperbranched Chains with Uniform Subchains and Controlled Locations of Cleavable Disulfide Linkages. *Macromolecules* **2014**, *47*, 650−658.
(37) Ryu, J. H.; Roy, R.; Ventura, J.; Thayumanavan, S. Redox-Sensitive Disassembly of Amphiphilic Copolymer Based Micelles. *Langmuir* **2010**, *26*, 7086−7092.


DOI: 10.1021/acs.macromol.8b01784
*Macromolecules* 2019, 52, 1173−1187

(38) Liu, S. Q.; Wiradharma, N.; Gao, S. J.; Tong, Y. W.; Yang, Y. Y. Bio-Functional Micelles Self-Assembled from a Folate-Conjugated Block Copolymer for Targeted Intracellular Delivery of Anticancer Drugs. *Biomaterials* **2007**, *28*, 1423−1433.
(39) Cuong, N. V.; Li, Y. L.; Hsieh, M. F. Targeted Delivery of Doxorubicin to Human Breast Cancers by Folate-Decorated Star-Shaped PEG-PCL Micelle. *J. Mater. Chem.* **2012**, *22*, 1006−1020.
(40) Sun, Y.; Yan, X. L.; Yuan, T. M.; Liang, J.; Fan, Y. J.; Gu, Z. W.; Zhang, X. D. Disassemblable Micelles Based on Reduction-Degradable Amphiphilic Graft Copolymers for Intracellular Delivery of Doxorubicin. *Biomaterials* **2010**, *31*, 7124−7131.
(41) Nojima, S.; Fujimoto, M.; Kakihira, H.; Sasaki, S. Effects of Copolymer Composition on the Crystallization and Morphology of Poly (ε-caprolactone)-*block*-Polystyrene. *Polym. J.* **1998**, *30*, 968−975.
(42) Shi, G. Y.; Yang, L. P.; Pan, C. Y. Synthesis and Characterization of Well-Defined Polystyrene and Poly (ε-caprolactone) Hetero Eight-Shaped Copolymers. *J. Polym. Sci., Part A: Polym. Chem.* **2008**, *46*, 6496−6508.
(43) Lee, R. S.; Li, H. R.; Yang, J. M.; Tsai, F. Y. Synthesis of Biodegradable Poly (trans-4-hydroxy-N-benzyloxycarbonyl-l-proline)-Block-Poly (ε-caprolactone) Copolymers and Micellar Characterizations. *Polymer* **2005**, *46*, 10718−10726.
(44) Riva, R.; Schmeits, S.; Jérôme, C.; Jérôme, R.; Lecomte, P. Combination of Ring-Opening Polymerization and "Click Chemistry": toward Functionalization and Grafting of Poly (ε-caprolactone). *Macromolecules* **2007**, *40*, 796−803.
(45) Oh, J. K.; Siegwart, D. J.; Matyjaszewski, K. Synthesis and Biodegradation of Nanogels as Delivery Carriers for Carbohydrate Drugs. *Biomacromolecules* **2007**, *8*, 3326−3331.
(46) Pinnel, P.; Mendez-Nelson, A.; Noh, S. M.; Nam, J. H.; Oh, J. K. Rapid and Tunable Reductive Degradation of Disulfide-Labeled Polyesters. *Macromol. Chem. Phys.* **2012**, *213*, 678−685.
(47) Li, L. W.; Lu, Y. Y.; An, L. J.; Wu, C. Experimental and Theoretical Studies of Scaling of Sizes and Intrinsic Viscosity of Hyperbranched Chains in Good Solvents. *J. Chem. Phys.* **2013**, *138*, 114908.
(48) Yasin, M.; Tighe, B. J. Polymers for Biodegradable Medical Devices: VIII. Hydroxybutyrate-hydroxyvalerate Copolymers: Physical and Degradative Properties of Blends with Polycaprolactone. *Biomaterials* **1992**, *13*, 9−16.
(49) Bogdanov, B.; Vidts, A.; Schacht, E.; Berghmans, H. Isothermal Crystallization of Poly (ε-caprolactone-ethylene glycol) Block Copolymers. *Macromolecules* **1999**, *32*, 726−731.
(50) You, J. H.; Choi, S. W.; Kim, J. H.; Kwak, Y. T. Synthesis and Microphase Separation of Biodegradable Poly (ε-caprolactone)-Poly (ethylene glycol)-Poly (ε-caprolactone) Multiblock Copolymer Films. *Macromol. Res.* **2008**, *16*, 609−613.
(51) Li, Y. L.; Zhu, L.; Liu, Z. Z.; Cheng, R.; Meng, F. H.; Cui, J. H.; Ji, S. J.; Zhong, Z. Y. Reversibly Stabilized Multifunctional Dextran Nanoparticles Efficiently Deliver Doxorubicin into the Nuclei of Cancer Cells. *Angew. Chem., Int. Ed.* **2009**, *48*, 9914−9918.
(52) Su, W.; Luo, X. H.; Wang, H. F.; Li, L.; Feng, J.; Zhang, X. Z.; Zhuo, R. X. Hyperbranched Polycarbonate-Based Multimolecular Micelle with Enhanced Stability and Loading Efficiency. *Macromol. Rapid Commun.* **2011**, *32*, 390−396.
(53) Wang, W.; Sun, H. L.; Meng, F. H.; Ma, S. B.; Liu, H. Y.; Zhong, Z. Y. Precise Control of Intracellular Drug Release and Anti-Tumor Activity of Biodegradable Micellar Drugs via Reduction-Sensitive Shell-Shedding. *Soft Matter* **2012**, *8*, 3949−3956.
(54) Shi, C. L.; Guo, X.; Qu, Q. Q.; Tang, Z. M.; Wang, Y.; Zhou, S. B. Actively Targeted Delivery of Anticancer Drug to Tumor Cells by Redox-Responsive Star-Shaped Micelles. *Biomaterials* **2014**, *35*, 8711−8722.
(55) Liu, J. Y.; Pang, Y.; Huang, W.; Zhu, Z. Y.; Zhu, X. Y.; Zhou, Y. F.; Yan, D. Y. Redox-Responsive Polyphosphate Nanosized Assemblies: a Smart Drug Delivery Platform for Cancer Therapy. *Biomacromolecules* **2011**, *12*, 2407−2415.
(56) Sun, H. L.; Guo, B. N.; Li, X. Q.; Cheng, R.; Meng, F. H.; Liu, H. Y.; Zhong, Z. Y. Shell-Sheddable Micelles Based on Dextran-SS-Poly (ε-caprolactone) Diblock Copolymer for Efficient Intracellular Release of Doxorubicin. *Biomacromolecules* **2010**, *11*, 848−854.
(57) Russo, A.; DeGraff, W.; Friedman, N.; Mitchell, J. B. Selective Modulation of Glutathione Levels in Human Normal versus Tumor Cells and Subsequent Differential Response to Chemotherapy Drugs. *Cancer Res.* **1986**, *46*, 2845−2848.
(58) Ko, N. R.; Oh, J. K. Glutathione-Triggered Disassembly of Dual Disulfide Located Degradable Nanocarriers of Polylactide-Based Block Copolymers for Rapid Drug Release. *Biomacromolecules* **2014**, *15*, 3180−3189.
(59) Sun, H. L.; Guo, B. N.; Cheng, R.; Meng, F. H.; Liu, H. Y.; Zhong, Z. Y. Biodegradable Micelles with Sheddable Poly (ethylene glycol) Shells for Triggered Intracellular Release of Doxorubicin. *Biomaterials* **2009**, *30*, 6358−6366.


DOI: 10.1021/acs.macromol.8b01784
*Macromolecules* 2019, 52, 1173−1187